Journal of Nanobiotechnology

RESEARCH

Open Access

Circ_0008315 promotes tumorigenesis and cisplatin resistance and acts as a nanotherapeutic target in gastric cancer

Yao Fei[1†], Danping Cao[1†], Yanna Li[1†], Zhixiong Wang[1], Runyu Dong[1], Menglin Zhu[1], Peng Gao[1], Xiaoming Wang[2], Juan Cai[3,4*] and Xueliang Zuo[1,3*]

Abstract

Introduction Cisplatin-based chemotherapy is one of the fundamental therapeutic modalities for gastric cancer (GC). Chemoresistance to cisplatin is a great clinical challenge, and its underlying mechanisms remain poorly understood. Circular RNAs (circRNAs) are involved in the pathophysiology of multiple human malignancies.

Methods High-throughput sequencing was performed to determine the differentially expressed profile of circRNA in GC tissues and cisplatin-resistant GC cells. Quantitative real-time polymerase chain reaction and Fluorescence in situ hybridization was utilized to confirm the dysregulation of circ_0008315 in GC tissues. To evaluate the prognostic significance of circ_0008315 in GC, we used Kaplan-Meier plot. The self-renewal ability of drug-resistant GC cell was verified through tumor sphere formation assay. GC organoids were constructed to simulate the tumor microenvironment and verified the function of circ_0008315 in cisplatin resistance of gastric cancer. In vivo evaluation was conducted using patient-derived xenograft models. Dual-luciferase reporter gene, RNA immunoprecipitation and miRNA pull-down assays were employed to investigate the molecular mechanisms of circ_0008315 in GC.

Results We revealed that a novel circRNA hsa_circ_0008315 was upregulated in GC and cisplatin-resistant GC cells. Elevated circ_0008315 was also observed in cisplatin-resistant GC organoid model. High circ_0008315 expression predicted unfavorable survival outcome in GC patients. Downregulation of circ_0008315 expression inhibited proliferation, mobility, and epithelial-mesenchymal transition of GC cells in vitro and in vivo. Reducing circ_0008315 expression in cisplatin-resistant GC organoid model reversed cisplatin resistance. Mechanistically, circ_0008315 modulated the stem cell properties of GC through the miR-3666/CPEB4 signaling pathway, thereby promoting cisplatin resistance and GC malignant progression. Furthermore, we developed PLGA-PEG nanoparticles targeting circ_0008315, and the nanoparticles could effectively inhibit GC proliferation and cisplatin resistance.

Conclusion Circ_0008315 exacerbates GC progression and cisplatin resistance, and can be used as a prognostic predictor. Circ_0008315 may function as a promising nanotherapeutic target for GC treatment.

[†]Yao Fei, Danping Cao and Yanna Li contributed equally to this work.

*Correspondence:
Juan Cai
caijuan1987@yeah.net
Xueliang Zuo
zuoxueliang0202@126.com

Full list of author information is available at the end of the article

Graphical Abstract

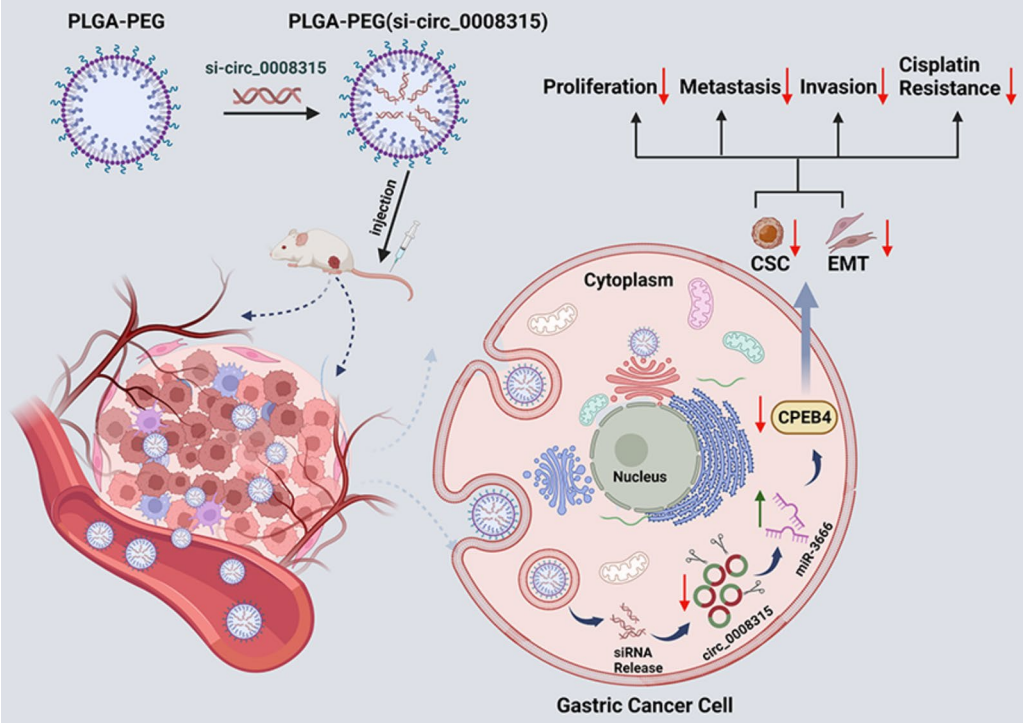

Keywords Gastric cancer, Circ_0008315, Cisplatin resistance, CPEB4, Nanoparticles

Introduction

Cancer is one of the most serious human health problems faced by modern society. As one of the most common tumors, gastric cancer (GC) has a critical impact on human health [1]. Tumor metastasis and chemoresistance are the central causes for GC relapse [2]. For advanced GC, chemotherapy is one of the most commonly used therapeutic methods. As one of the chemotherapy drugs, cisplatin (CDDP) is extensively used to treat advanced GC [3]. However, chemoresistance to CDDP remains a great clinical challenge [4]. CDDP resistance is mediated by aberrant drug transportation, enhanced detoxification, dysregulated apoptosis, and defective DNA repair capability [5]. Exploring the molecular mechanisms of CDDP resistance is of great significance for developing effective GC treatment strategies.

CircRNAs, as a novel type of non-coding RNA, play crucial roles in a variety of biological pathophysiological processes [6, 7]. CircRNAs are involved in the commands of tumorigenesis and cancer progression [8, 9]. It has been demonstrated that circRNAs could regulate gene expression at both the transcriptional and post-transcriptional levels simultaneously [10]. CircRNAs can competitively bind microRNAs (miRNAs) and regulate the expression level of miRNA downstream target genes, thus affecting GC progression. For instance, circRHOBTB3 functions as a competing endogenous RNA (ceRNA) for miR-654-3p and inhibits GC growth by activating the p21 signaling pathway [11]. CircAKT3 upregulates PIK3R1 to enhance CDDP resistance in GC via miR-198, and inhibits the apoptosis of GC cells in vivo and in vitro [12]. Hsa_circ_0008315 is located on chromosome 5 and derived from *RASGRF2*. It has been reported that circRASGRF2 expression is upregulated in hepatocellular carcinoma, and high circRASGRF2 expression is associated with an unfavorable prognosis [13]. However, the role of circ_0008315 in GC remains unclear. Herein, we constructed GC organoids to simulate the tumor microenvironment in vivo to detect the expression of circ_0008315 and its impact on cisplatin resistance. We demonstrated that circ_0008315 could sponge miR-3666 to affect the expression of CPEB4, thereby promoting GC progression. GC patients with high circ_0008315 expression suffered from poor survival outcomes. Furthermore, circ_0008315 could regulate the stem cell properties of GC cells through the miR-3666/CPEB4 axis to promote CDDP resistance and GC malignant progression, providing a nanotherapeutic candidate for GC patients.

Materials and methods

Specimen collection

The clinical specimens including GC tissue samples (N=40) and the matched adjacent nontumorous tissues samples (N=40) were collected from GC patients who underwent radical gastrectomy at the First Affiliated Hospital of Wannan Medical College. Patients receiving preoperative radiotherapy or chemotherapy before collection were excluded. All tissue specimens have obtained written informed consent from the patients before separation, and the samples are immediately stored in liquid nitrogen for further analysis after surgery. This study was approved by the Ethics Committee of the First Affiliated Hospital of Wannan Medical College.

Cell culture and transfection

We mixed fetal bovine serum (FBS; Invitrogen, USA) at a concentration of 10% into RPMI-1640 medium (Gibco, USA), while adding 100U/ml penicillin and 100 μg/ml streptomycin, used for cultivating human GC cell lines (HGC-27, AGS, MKN-45, and MKN-28) and normal gastric epithelial cell line GES-1. The MKN-45/CDDP and HGC-27/CDDP cell lines were established as previously reported [14]. To put it simply, after the passage of MKN-45 and HGC-27 cells was completed, CDDP was added to the medium for 48 hours. The concentration of CDDP started from 1 μM. when the cells grew stably, the concentration of CDDP increased gradually, and the final concentration was 10 μM. To maintain the drug-resistant phenotype of the MKN-45/CDDP and HGC-27/CDDP cells, 0.8 μg/ml of CDDP (Sigma-Aldrich, USA) was added to the RPMI-1640 medium (Gibco, USA). All cells reproduced in 37℃ humid incubator containing 5% carbon dioxide. The transfection reagent was Lipofectamine^{TM}3000 (Invitrogen). The siRNAs and overexpression plasmid of circ_0008315 were designed and constructed by GenePharm (China). The siRNA sequences are as follows: si-circ_0008315#1: 5'-GUCCACCAGCAGUCCUAGATT-3', si-circ_0008315#2: 5'-CCACCAGCAGUCCUAGAGUTT-3', si-KLF7#1: 5'-GUUGGCUAGUUAUAGUAUATT-3', si-KLF7#2: 5'-GGGUGCCGGAAAGUUUAUATT-3', si-KLF7#3: 5'-GCUCUUCUCUAGACAGCUATT-3', si-KLF7#4: 5'-CUCCACAUGAAGAGACAUATT-3'.

RNase R digestion and actinomycin D assays

Total RNA was collected from GC tissues and cells by TRIzol reagent (Invitrogen). The extracted total RNA of GC cell lines was mixed with 3 U/mg of RNase R for 15 min at 37 °C. The stability of circ_0008315 and RASGRF2 were detected by agarose gel electrophoresis. MKN-45 cells were treated with actinomycin D for 0 h, 4 h, 8 h, 12 h and 24 h, respectively, before RNA extraction. Detecting the expression of circ_0008315 and RASGRF2 through RT-qPCR to assess its stability.

FISH and IF assays

Cy3-labeled circ_0008315 and FAM-labeled miR-3666 probes were designed and synthesized by GenePharm. Therefore, we chose a Fluorescent In Situ Hybridization Kit from GenePharm to measure the fluorescent signals of the probe. The acquisition of fluorescence images was completed by the Zeiss confocal laser scanning microscope. The probe sequence of hsa_circ_0008315 is 5'-GACTGCTGGTGGACTCCCATGTCCCTCTAGGACTGCTGGTGGACTCCCATGCAGACTCTAGGACTGCTGGTGGA-3'. The probe sequence of hsa_miR_3666 is 5'-TCGGCATCTACACTTGCACTG-3'.

For IF assays, we placed the cells in 4% paraformaldehyde for 30 min to fix their components, and used PBS containing 0.5% Triton X-100 to penetrate the cell membranes and nuclear membranes, then sealed with 3% bovine serum albumin, and incubated with E-cadherin (#3195, Cell Signaling Technology, USA), N-cadherin (#5741, Cell Signaling Technology), Ki-67 (#34330, Cell Signaling Technology), TUNEL (#25879, Cell Signaling Technology) primary antibodies overnight at 4℃. After that, the cells were incubated with HRP fluorescent secondary antibodies at room temperature for 2 h to give the immune complex fluorescent signals. Photographs were taken under fluorescence microscope (Nikon, Japan).

Total RNA extraction, nucleocytoplasmic separation, and RT-qPCR assays

Total RNA was extracted from tissues and cultured cells. For the detection of circ_0008315 expression levels, cDNA was synthesized with TransScript RT Enzyme (GeneSeed, China). RT-qPCR was performed with SYBR Green Master Mix (GeneSeed) according to the manufacturer's guide. For miRNA, cDNA was synthesized using a MiRcute Enhanced miRNA cDNA First-Strand Synthesis Kit (Tiangen, China). Subsequently, the real-time PCR of cDNA was executed on a QuantStudio Dx system (Applied Biosystems, Singapore). Standardization was achieved through $2^{-\Delta\Delta ct}$ method compared the target mRNA with the mRNA of an internal controls (GAPDH or U6). The PARIS™ Kit (Invitrogen) was applied to pick up nuclear and cytoplasmic RNA in cells according to the manufacturer's protocols. The relative expression of circ_0008315 in the nuclear and cytoplasmic fractions was gauged by RT-qPCR. RT-qPCR amplification was carried on using the following primers: circ_0008315: forward: 5'-GGACAATGCCCACTGCTCTG-3'; reverse: 5'-TGCAGACTCTAGGACTGCTGGT-3'; CPEB4: forward: 5'-GTTCACAGCCACTTGACCCA-3'; reverse: 5'-ATCAATCCCAGCGTAGCACA-3'; GAPDH: forward: 5'-GAACGGGAAGCTCACTGG-3'; reverse: 5'-GCCTGCTTCACCACCTTCT-3'. The RT-qPCR primers for miR-3666 and U6 were designed and synthesized by RiboBio (China).

Cell proliferation assay

Cell counting kit-8 (CCK-8, Bestibo, China) was used to measure the proliferative capacity of GC cell lines. Transfected GC cells were seeded into a 96-well plate with 2000 cells per well and cultured at the indicated time (24 h, 48 h, 72 h and 96 h). Seeded cells were incubated for 2 h with the CCK-8 reagent before the detection of absorbance at 450 nm by use of a microplate reader.

5-Ethynyl-2′-deoxyuridine (EdU) incorporation assay

A Cell-light EdU DNA Cell Proliferation Kit (Guangzhou, China) was used for EdU analysis, which indicated GC cell proliferation. After incubation with 50 mM EdU for 2 h, GC cells were fixed in 4% paraformaldehyde and stained with Apollo staining solution. Subsequently, the nucleus was stained with Hoechst33342 for half an hour. Proliferative positive cells were photographed and counted under a microscope (Nikon, Japan).

Cell apoptosis assay

For apoptosis analysis, the GC cells were harvested and assesses for apoptosis using Annexin V-FITC/PI double staining Apoptosis Detection Kit (Bestbio, China). The proportion of apoptotic GC cells was detected and analyzed by a flow cytometer (Beckman, USA).

Cell cycle assay

The transfected cells were harvested and resuspended into cell suspension after cultured for 48 h. The cells were washed with cold phosphate-buffered saline (PBS) twice and fixed with cold 75% ethanol for 2 h at 4℃. After that, the cells were stained with PI containing RNAase for 30 min and washed with PBS for three times. Finally, the cell cycle was measured by flow cytometry (Beckman, USA), and the data analysis was conducted by Modifit software.

Transwell assay

Transwell assays were used for invasion capability detection. Specifically, the small chambers were first coated with 100 uL of Matrigel (Invitrogen) for a 30 min incubation, 4×105 transfected GC cells were suspended in 200 μL Serum-free medium and placed to upper chamber of 24-well transwell plates (8 μm-poresize, Corning, USA), and 600 μL of complete medium containing 15% FBS was added to the bottom chambers. After 24 h co-culture in the incubator, the cells on the lower surface of membrane were fixed in 4% paraformaldehyde, stained by 0.1% crystal violet. The stained cells were then counted under Nikon light microscope (Nikon, Japan).

Wound healing assay

GC cells were seeded and transfected in 6-well plates and cultured until they reached complete confluency as a monolayer. Use a 20 μL pipette tip to slowly cut a straight line in the well. The wells were then washed three times with PBS and replaced with serum-free medium for 24 h. The images were recorded under an electron microscope, and the percentage of wound healing was calculated by ImageJ.

Sphere formation assay

The self-renewal ability of drug-resistant GC cell was verified through tumor sphere formation assay. Digested cells were seeded in ultra-low-attachment 6-well plates (Corning, USA) at an appropriate density with the stem cell medium. Each well was checked every 3 days by light microscopy. The quantity of tumor spheres of 100 μm or more was counted 7 days later. Images of tumor spheres were taken by microscope, and tumor size was measured using ImageJ software.

Western blotting assay

We extracted total proteins from GC cells and tissues using lysis buffer containing protease inhibitors. The extracted protein was transferred to the PVDF membrane through SDS-PAGE electrophoresis. After blocking in TBST buffer with QuickBlock Western (Beyotime, China), the membranes were incubated with the primary antibodies at 4 ℃ overnight to form an antigen antibody complex of the target protein. Subsequently, membranes was cultured with the secondary antibodies at room temperature for 2 h, allowing the target protein to be detected. After each antibody binding, the membranes should be cleaned three times with TBST. The marks were visualized with an enhanced chemiluminescence detection system with Chemiluminescence HRP Substrate (Millipore, USA). The primary antibodies containing the following: CPEB4 (#25342-1-AP, Proteintech, China), E-cadherin (#3195, Cell Signaling Technology), N-cadherin (#5741, Cell Signaling Technology), Vimentin (#4267, Cell Signaling Technology), CD44(#A21919, ABclonal), CD133(#A12711, ABclonal, China), GAPDH (# AB181602, Abcam, USA).

Dual-luciferase reporter gene assay

GC cells were seeded into 24-well plates for dual-luciferase reporter gene assays. Using the Lipofectamine™ 3000 as a transfection reagent, cells at a confluence from 60 to 70% were cotransfected with wild-type or mutant hsa_circ_0008315 3'UTR or CPEB4 3'UTR reporter plasmids as well as miR-3666 mimics or negative controls. After 24 h of incubation, the activity of firefly and renilla luciferase was detected using the Dual-Luciferase Reporter Assay System. The ratio of the two was the relative activity of luciferase.

Lentivirus transfection and stable cell line construction

Lentiviruses overexpressing circ_0008315 and lentiviral-based small hairpin RNAs (shRNAs) targeting circ_0008315 and were designed and established by GenePharma. The shRNA sequences are as follows: sh-circ_0008315: 5'-GTCCACCAGCAGTCCUAGATT-3'. MiR-3666 mimics and inhibitors were purchased from RiboBio.

Xenograft animal assay and lung metastasis model

Subcutaneously inoculated 5×10^6 GC cells into the lateral abdomen of each nude mouse (4 weeks of age, male, BALB/c). Every three days, we measured the length and width of subcutaneous tumors and calculated their volume using the formula: tumor volume = (length × width^2) / 2. The maximum allowed tumor diameter of 20 mm in any extent was never exceeded. After one month of feeding, the subcutaneous tumor was removed and calculated. For metastasis model, 2×10^6 GC cells were inoculated into nude mice via tail vein. After 8 weeks, the mice were monitored by bioluminescence imaging using the Aniview Imaging System (Biolight Biotechnology, China). The lungs were harvested and fixed in 4% paraformaldehyde for further analysis. Sections were subjected to histopathological analysis. For mice that required CDDP treatment, we injected CDDP into their tail vein every two days at a concentration of 2.5 mg/kg. All animal experiments were approved by the Ethics Committee of the First Affiliated Hospital of Wannan Medical College.

PDX mouse model

We constructed PDX models of GC using NOD/SCID and BALB/c mice. Briefly, primary tumor tissues from GC patients undergoing gastrectomy were preserved in 100 μl of 50% Matrigel (BD Biosciences, USA) in 100 μl of ice-cold culture media supplemented with 1% penicillin/streptomycin. After that, NOD/SCID mice received subcutaneous implants of the tissue samples. Engrafted tumors were removed after they reached a size of 1–2 cm^3 and were then spliced for further injections into BALB/c nude mice. When the engrafted tumor volume reached around 200 mm^3, the Saline, Free si-circ_0008315#1, PLGA-PEG(si-circ_0008315#1)NPs, and PLGA-PEG(si-NC)NPs were injected twice a week at a dose of 200 mg/kg via tail vein. Tumor volume and weight were measured, and the tumors were processed for further experiments.

Cell viability assay

The cell viability was assessed by CCK-8 assays at various time points in 96-well dishes to measure the cytotoxicity of CDDP. Briefly, GC sensitive cells and GC CDDP-resistant cells were seeded in 96-well plates at 4×10^3 cells/well for 24 h. All of them were treated with different concentrations of CDDP (0, 0.5, 1, 2,4,8, 16 μM) in the following. Briefly, the 10 uL CCK-8 solution (Best-Bio, China) was added into each well and cultured at the condition of 5% CO2 and 37℃ for 2 h. The half maximal inhibitory concentration (IC50) and cell viability ware determined and analyzed at the absorbance of 450 nm by applying a microplate reader (Thermo scientific, United States).

Colony formation assay

About 1000 cells were seed in 6-well dishes and treated with CDDP at the indicated concentrations for 48 h. All of them were cultured in 1640 medium at the condition of 5% CO2 and 37℃ for 2 weeks. All the cells were harvested after PBS buffer washed, fixed with 4% paraformaldehyde for 30 min, and dyed with 1% crystal violet dye solution. The number of colonies was photographed and calculated.

IHC assay

Tumor specimens were fixed with 4% paraformaldehyde, paraffin embedding, sectioning, dewaxing, and staining according to instructions. Ki-67 (#34330, Cell Signaling Technology), E-cadherin (#3195, Cell Signaling Technology), N-cadherin (#5741, Cell Signaling Technology), and CPEB4 (#25342-1-AP, Proteintech) antibodies were dropped onto tissue slices and incubated overnight, followed by the addition of secondary antibodies for incubation to bind to the primary antibodies. The conditions of the stained sections were observed and recorded under a microscope.

Human organoid culture

Human GC tissues were obtained from patients undergoing surgery at The First Affiliated Hospital, Yijishan Hospital of Wannan Medical College. The patients did not undergo any other anti-tumor treatment before the surgery. The patients had already signed an informed consent form before surgery. We referred to previous methods for cultivating GC organoids [15]. Organoids were passaged once every 15 days at a ratio of 1:2/1:3. 72 h after passaging, we used CDDP to treat the corresponding groups of organoids.

RIP assay

The RIP assay was performed in MKN-45 and HGC-27 cells using the Magna RIP RNA-Binding Protein Immunoprecipitation Kit (Millipore) in accordance with the manufacturer's protocol. First, around 1×10^7 cells were lysate with RIP lysate containing protease and RNase inhibitor (Millipore) and incubated overnight with anti-AGO2 antibody (Abcam, # AB186733) or non-specific IgG antibody (Abcam) at 4℃. The appropriate amount

of protease K was added to the sample and incubated at 55℃ for 30 min. After elution, immunoprecipitated RNAs were obtained and analyzed by RT-qPCR.

Biotin-labeled miRNA pull-down assay

The final concentration of 3' end biotinylated miR-3666 mimic or control biotin-RNA (RiboBio) was adjusted to 20nmol/L. And then the experimental group and the control group were transfected into cells for 1 day, respectively. The biotin-coupled RNA complex was isolated by incubating the cell lysate containing streptavidin-coated magnetic beads (Ambion, USA). The abundance of circ_0008315 in bound fractions was evaluated by RT-qPCR analysis.

Preparation of PLGA-PEG(si-circ_0008315#1)NPs

PLGA-PEG(si-circ_0008315#1)NPs were prepared by the double emulsion solvent diffusion method. Circ_0008315 was dissolved in DEPC water and then mixed with spermidine (Sigma-Aldrich) in an 8:1 N/P ratio (the ratio of polyamine groups to siRNA phosphate groups). The resulting mixture was cultivated at room temperature for 15 min to attain si-circ_0008315#1/arginine compound. PLGA-PEG-COOH (10 mg; DaiGang Biology, China) was dissolved in 500 μL methylene chloride (Aladdin, China). The dichloromethane solution was added to si-circ_0008315#1/arginine complex by drops in an ice bath and mixed and emulsified with ultrasonic probe apparatus. The obtained primary emulsion was further dripped into 4 ml water containing 2.5% polyvinyl alcohol (Aladdin) and emulsified with a probe for 1 min. We stirred the obtained emulsion at room temperature for 4 h to remove the organic solvent as much as possible. The blend was centrifuged for 15 min to collect NPs, and then DEPC washed NPs 2 times. We used Zetaview nanoparticle tracking analysis (NTA) to investigate the particle size, zeta potential, and PDI of NPs. The samples were then dropped into the copper mesh and dried at room temperature to obtain TEM NPs images.

In vivo antitumor efficacy and toxicity evaluation of NPs

To investigate the inhibitory effect of PLGA-PEG(si-circ_0008315#1)NPs on growth in vivo, a PDX tumor model was established as described above. When the tumor grew to 200 mm^3, saline, free si-circ_0008315#1, PLGA-PEG(si-NC)NPs, and PLGA-PEG(si-circ_0008315#1)NPs were injected into the mice twice a week at a dose of 200 mg/kg via the caudal vein. For further investigation of the suppressive effect of PLGA-PEG(si-circ_0008315#1)NPs on GC CDDP resistance in vivo, CDDP-resistant xenograft models were established by injecting of MKN-45/CDDP cells into the flanks of nude mice. When the tumor volume reached about 200 mm^3, saline, free si-circ_0008315#1, PLGA-PEG(si-circ_0008315#1)NPs and PLGA-PEG(si-NC)NPs were injected into mice via tail vein. The mice were executed five weeks later, and tumor weight and volume were recorded. At the same time, the heart, liver, kidney, spleen, and lung were seperated and fixed with 4% paraformaldehyde, followed by H&E staining. Moreover, the levels of mice blood ALT, AST, Cr, and BUN were analyzed to examine the hepatic and renal toxicity of PLGA-PEG(si-circ_0008315#1)NPs.

Statistical analysis

The experimental results were further analyzed using graphpad prism 7, and the obtained data were expressed in mean ± SD. Student's *t* test and one-way analysis of variance were used for significance analysis. The survival data of GC patients were analyzed by log-rank test, and the survival curve was produced by Kaplan-Meier plot. Spearman correlation coefficient analysis was utilized to estimate the correlation among circ_0008315, miR-3666, and CPEB4 levels in GC tissues. It is considered as statistically significant when $p < 0.05$.

Results

Identification of a novel circRNA hsa_circ_0008315 in CDDP-resistant GC cells

To investigate the molecular mechanism underlying metastasis and CDDP resistance in GC, we analyzed the differentially expressed circRNAs in 3 paired GC tissues and adjacent tissues by high-throughput RNA-seq (Fig. 1A). Moreover, we conducted RNA-seq analysis of CDDP-resistant cells and the corresponding parental CDDP-sensitive cells (Fig. 1B, Additional file 1: Fig. S1A and B). We took the intersection of these RNA-seq results and determined the overlapped genes. We found a novel circRNA hsa_circ_0008315 that was located on chromosome 5. RNA-seq analysis showed that circ_0008315 was significantly upregulated in GC tissues and CDDP-resistant cells. RNA isolation and quantitative real-time polymerase chain reaction (RT-qPCR) was employed to determine the expression of circ_0008315 using 40 pairs of matched GC and adjacent tissue samples. As shown in Fig. 1C, the expression of circ_0008315 in GC tissues was significantly upregulated than that in normal tissues. In CDDP-resistant cells, Circ_0008315 expression level increased more obviously (Fig. 1D). Compared with normal gastric epithelial cell GES-1, circ_0008315 increased in all 4 GC cell lines, consistently (Fig. 1E). Based on annotation from circBase, we found that circ_0008315 was generated from exons 16–17 of the *RASGRF2* gene with a length of 216 bp (Fig. 1F). Sanger sequencing results confirmed the head-to-tail splicing of circ_0008315 (Fig. 1G). Agarose gel electrophoresis assays showed that the divergent primers could amplify circ_0008315 in cDNA, while no amplification was

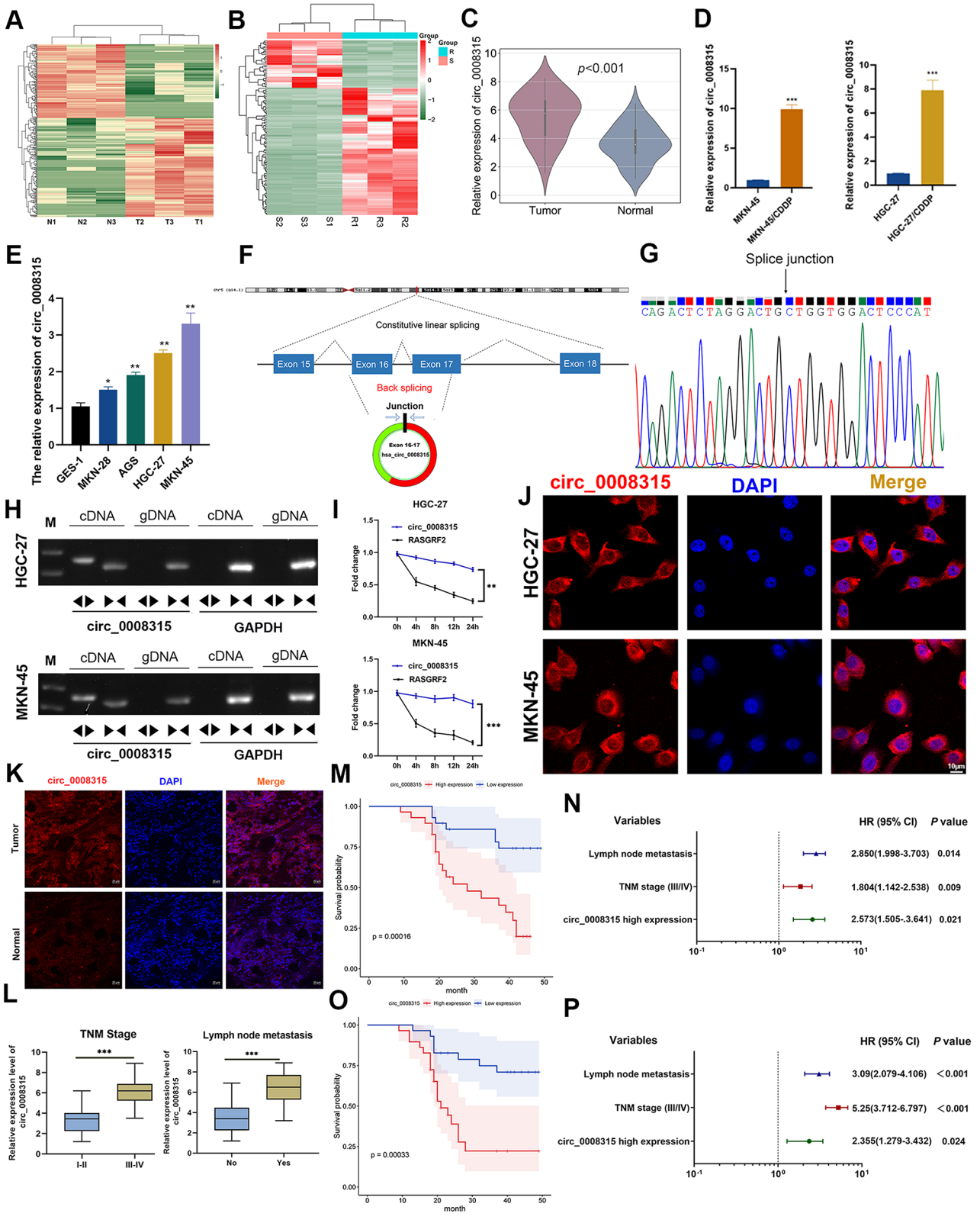

Fig. 1 (See legend on next page.)

(See figure on previous page.)

Fig. 1 Circ_0008315 is upregulated in GC tissues and CDDP-resistant GC cells. **A** Differential expression heatmap of circRNAs between GC tissues and corresponding normal tissues. **B** Differential expression heatmap of circRNA between CDDP-resistant and non-resistant GC cells. **C** Detection of circ_0008315 expression in GC tissues and normal gastric epithelial tissues using RT-qPCR. **D** The circ_0008315 expression levels were examined by RT-qPCR in CDDP-resistant cells (MKN-45/CDDP, HGC-27/CDDP) and parental CDDP-sensitive cells (MKN-45 and HGC-27). **E** The circ_0008315 expression levels in GES-1 and GC cells. **F**, **G** The circ_0008315 was back-spliced by exon 16 and 17 of RASGRF2 and verified by Sanger sequencing. **H** Agarose gel electrophoresis showed that only divergent primers amplified circ_0008315 in cDNA. GAPDH served as a negative control. **I** RT-qPCR for the abundance of circ_0008315 and RASGRF2 mRNA in HGC-27 and MKN-45 cells treated with Actinomycin D at the indicated time points. **J** FISH results showing the localization of circ_0008315 in GC cells. Nuclei were stained with DAPI. **K** FISH experiment indicated that the expression level of circ_0008315 in GC tissues was significantly upregulated compared to normal tissues. **L** The expression level of circ_0008315 in stage III-IV patients was higher than that in stage I-II patients (left panel). Expression levels of circ_0008315 were compared between patients with and without lymph node metastasis (right panel). **M**, **O** Kaplan-Meier curves showed the correlation between the expression of circ_0008315 and overall survival disease-free survival. **N** Multivariate analyses of the independent risk factors for overall survival. The relevant 95% confidence intervals (CI) and hazard ratios (HR) are shown. **P** Multivariate analyses of the independent risk factors for disease-free survival. The relevant 95% CI and HRs are shown. *p < 0.05; **p < 0.01; ***p < 0.001

detected in genomic DNA, suggests that circ_0008315 was indeed a circRNA (Fig. 1H). After treatment with actinomycin D, the half-life of circ_0008315 was much longer than that of the linear RASGRF2, indicating that circ_0008315 was highly stable (Fig. 1I). Agarose gel electrophoresis experiment showed that circ_0008315 was more resistant to RNase R-mediated digestion than linear RASGRF2 (Additional file 1: Fig. S1C). Expression levels of circ_0008315 from the nuclear and cytoplasmic fractions of HGC-27 and MKN-45 cells were evaluated using RT-qPCR, and the results showed that circ_0008315 was predominantly located in cytoplasm (Additional file 1: Fig. S1D and E). RNA fluorescence in situ hybridization (FISH) confirmed that circ_0008315 was mainly localized in the cytoplasm (Fig. 1J). These results demonstrated that circ_0008315 harbored a loop structure and was upregulated in GC tissues and CDDP-resistant GC cells.

Circ_0008315 was upregulated in GC tissues and predicted poor survival

Results of the FISH assays confirmed the upregulation of circ_0008315 (Fig. 1K). RT-qPCR was used to analyze the expression levels of circ_0008315 in GC, and a total of 40 GC patients were divided into circ_0008315^{low} and circ_0008315^{high} groups according to the median expression level. High circ_0008315 expression level was correlated with poor tumor differentiation, advanced tumor stage, microvascular invasion, and lymph node metastasis (Additional file 2: Table S1). Expression level of circ_0008315 was markedly upregulated in GC patients at TNM stages III-IV and GC patients with lymph node metastasis (Fig. 1L). Kaplan-Meier survival plots showed that GC patients with high circ_0008315 expression level had a short overall survival (OS) and disease-free survival (DFS) than GC patients with low circ_0008315 expression (Fig. 1M and O). Lymph node metastasis, tumor TNM stage, and circ_0008315 expression level were found to be independent risk factors for OS and DFS in GC patients (Fig. 1N and P, Additional file 2: Table S2 and Table S3). These data demonstrated that circ_0008315 was upregulated in GC tissues and high circ_0008315 expression predicted unfavorable survival outcomes.

Circ_0008315 enhanced proliferation and repressed apoptosis of GC cells

To explore the biological functions of circ_0008315 in GC, we performed loss- and gain-of-function experiments. Two siRNAs (si-circ_0008315#1 and si-circ_0008315#2) were designed to knock down the expression of circ_0008315 in HGC-27 and MKN-45 cells. RT-qPCR showed that si-circ_0008315#1 and si-circ_0008315#2 significantly inhibited the expression of circ_0008315, and the *RASGRF2* mRNA expression remained unchanged (Fig. 2A). The cell viability was reduced by depletion of circ_0008315 in MKN-45 and HGC-27 cell lines according to CCK-8 assays (Fig. 2B). Similarly, the results of EdU assay revealed that circ_0008315 knockdown apparently decreased the proliferation of MKN-45 and HGC-27 cells (Fig. 2C). Moreover, the knockdown of circ_0008315 can lead to increased apoptosis of MKN-45 and HGC-27 cells (Fig. 2D). Compared to si-NC group, the contents of MKN-45 and HGC-27 cells that stagnated in G1 phase were higher in circ_0008315 knockdown group (Fig. 2E). These findings indicated that circ_0008315 could increase proliferation and attenuate apoptosis of GC cells. In contrast, overexpression of circ_0008315 significantly enhanced the proliferative capabilities of AGS and MKN-28 cells (Additional file 1: Fig. S2A-D).

Circ_0008315 promoted migration and invasion of GC cells

Subsequently, the effect of circ_0008315 in regulating the biological function of GC cells was detected. From transwell assays, it could be seen that invasion of HGC-27 and MKN-45 cells was alleviated in si-circ_0008315#1 and si-circ_0008315#2 groups (Fig. 2F). Besides, wound healing assays showed that circ_0008315 knockdown remarkably inhibited wound proportion in MKN-45 and HGC-27 cells (Fig. 2G). Additionally, ectopic expression of circ_0008315 in GC cells significantly facilitated cell invasion and migration (Additional file 1: Fig. S3A and B). These data indicated that circ_0008315 contributed to GC cell migration and invasion.

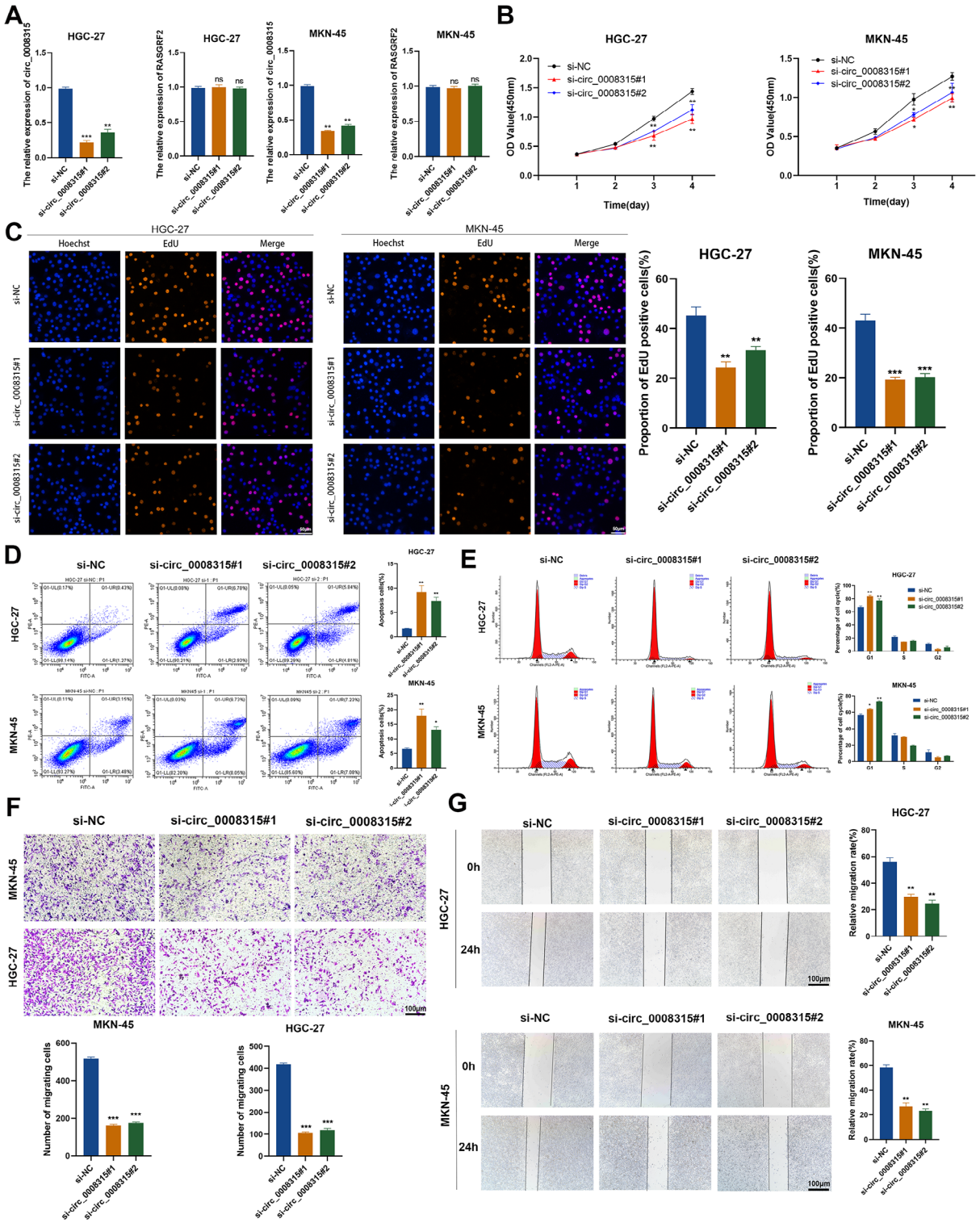

Fig. 2 Knockdown of circ_0008315 inhibits the proliferation and migration of GC cells. **A** RT-qPCR analysis of circ_0008315 and linear RASGRF2 expression levels after transfected with si-NC, si-circ_0008315#1 and si-circ_0008315#2 plasmids. **B**, **C** CCK-8 assay and EdU staining were performed to assess proliferation ability of cells transfected with si-NC, si-circ_0008315#1 and si-circ_0008315#2 plasmids. Scale bars, 50 mm. **D** Flow cytometry was used to analyze the effect of circ_0008315 knockdown on GC cell apoptosis. **E** Cell cycle assay results showed that circ_0008315 knockdown could induce G1 phase arrest of MKN-45 and HGC-27 cells. **F**, **G** The migration and invasion ability of MKN-45 and HGC-27 cells after circ_0008315 knockdown was detected by transwell and wound healing assays. Scale bars, 100 μm. We had repeated all the experiments at least three times and expressed the final results as mean ± SD. *p < 0.05; **p < 0.01; ***p < 0.001; ns indicates not significant

Circ_0008315 promoted epithelial-mesenchymal transition (EMT) of GC cells

Accumulating evidence has demonstrated that EMT endows epithelial cells with their migratory and invasive abilities, notably in cancer metastasis processes. To investigate the association between circ_0008315 and EMT, we performed multiple experiments to analyze the effects of circ_0008315 on EMT markers. As shown in Fig. 3A, circ_0008315 knockdown resulted in the transformation of MKN-45 cells to epithelial phenotype. In contrast, overexpression of circ_0008315 led to the generation of fusiform mesenchymal cells in MKN-28 cells compared to the control cells with an epithelioid phenotype. According to the results of western blotting, it can be seen that the content of mesenchymal markers N-cadherin and Vimentin decreased in the circ_0008315 knockdown group compared with the si-NC group, while the content of epithelial marker E-cadherin was higher. Whereas, circ_0008315 overexpression in GC cells exhibited the opposite effects (Fig. 3B). Compared to control cells, immunofluorescence (IF) showed that knockdown of circ_0008315 in MKN-45 cells resulted in a cobblestone cellular morphology and shrinkable F-actin fiber. In contrast, MKN-28 cells with circ_0008315 overexpression had an elongated appearance and morphology of F-actin fibers (Fig. 3C). Additionally, IF staining confirmed that circ_0008315 knockdown in MKN-45 cells elevated E-cadherin expression and decreased N-cadherin expression, whereas circ_0008315 overexpression reduced E-cadherin level and increased N-cadherin

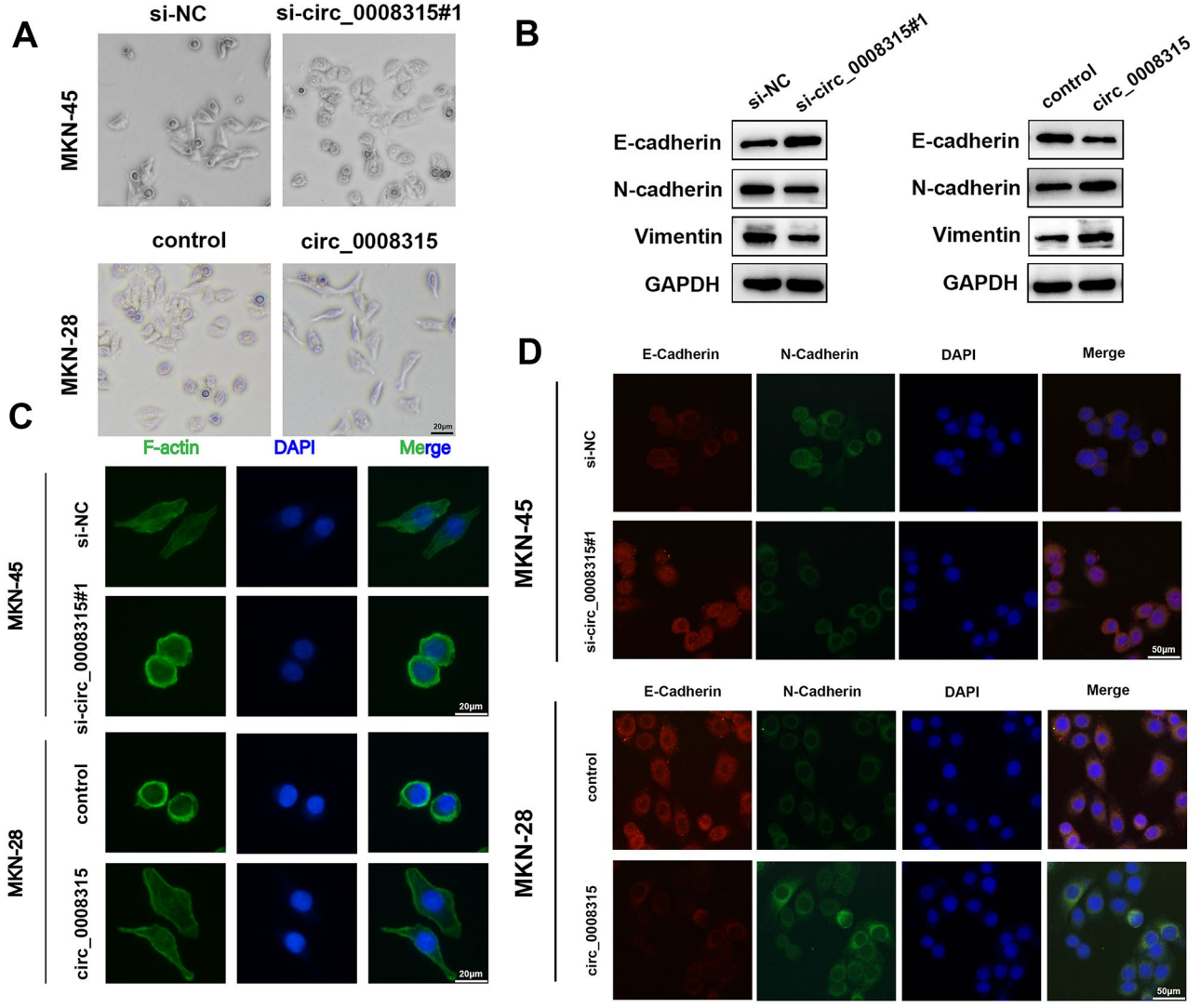

Fig. 3 Circ_0008315 promotes EMT in GC cells. **A** Morphological changes in MKN-45 cells with circ_0008315 knockdown and circ_0008315 overexpressed MKN-28 cells. **B** Western blotting assay was conducted to evaluate the effect of circ_0008315 knockdown or overexpression on the levels of E-cadherin, N-cadherin, Vimentin and Snail. **C** IF assay showing the cell morphology and f-actin apparatus of circ_0008315 knockdown or overexpressed GC cells. D The effect of knockdown or overexpression circ_0008315 on E-cadherin and N-cadherin in MKN-45 and MKN-28 cell lines detected by IF assay

expression in MKN-28 cells (Fig. 3D). Together, circ_0008315 was demonstrated to induce EMT in GC.

Circ_0008315 sponged miR-3666 in GC cells

Given that circ_0008315 was mainly located in the cytoplasm, we attempted to explore whether circ_0008315 could bind to miRNAs. As is shown in Fig. 4A, we analyzed the sequence of circ_0008315 using TargetScan, miRCode, miRDB, and starBase. We identified four candidate miRNAs by overlapping the prediction results, including miR-17-5p, miR-20b-5p, miR-3666, and miR-301b-3p. Next, we conducted RNA immunoprecipitation (RIP) with an antibody against AGO2 in MKN-45 and AGS cells. RIP results showed that circ_0008315 was significantly enriched by AGO2 antibody (Fig. 4B), suggesting that circ_0008315 may act as a binding platform for AGO2 and miRNAs. Notably, probes against circ_0008315 were utilized to analyze the four candidate miRNAs. We found a significant enrichment of miR-3666 compared to the controls, while the other miRNAs had no significant enrichment (Fig. 4C). We then generated a mutant sequence of circ_0008315 that could not bind miR-3666 (Fig. 4D). The luciferase experiment demonstrated that miR-3666 mimics could significantly diminished the luciferase activity of GC cells that transfected with wild-type circ_0008315 sequence, but not transfected with mutant circ_0008315 (Fig. 4E). FISH assays revealed the colocalization of circ_0008315 and miR-3666 in the cytoplasm of GC cells (Fig. 4F). Moreover, the expression of miR-3666 was decreased in GC cells and tissues (Fig. 4G and H). Furthermore, a reverse correlation was identified between circ_0008315 and miR-3666 expression levels (Fig. 4I). These findings indicated that circ_0008315 could sponge miR-3666 in GC.

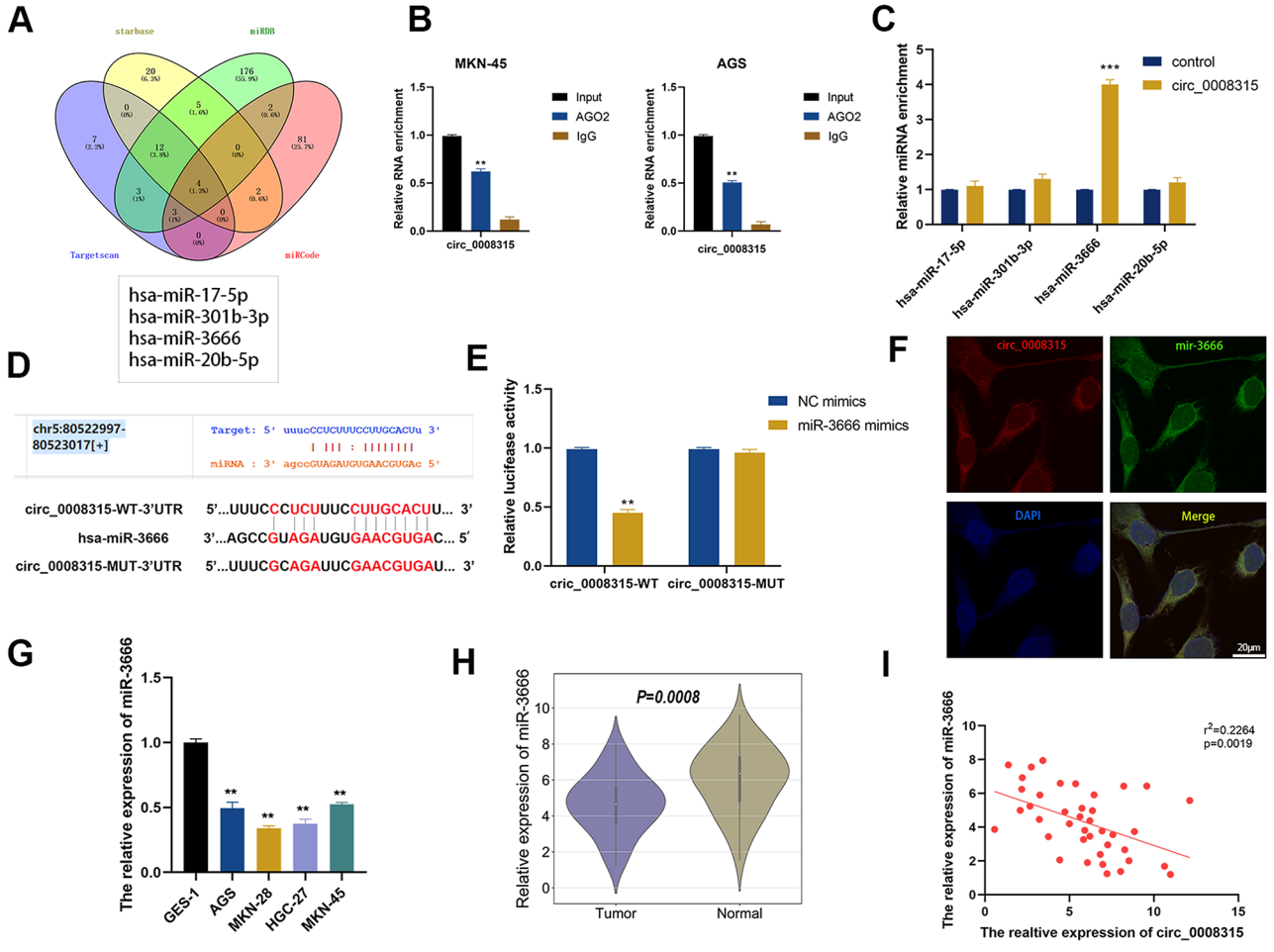

Fig. 4 Circ_0008315 could sponge miR-3666 in GC cells. **A** Venn diagram showing the prediction of circ_0008315 binding mRNAs from 4 databases. **B** Endogenous circ_0008315 was efficiently pulled down by anti-AGO2. **C** Biotin-labeled miRNA pull-down assay showed that circ_0008315 was only efficiently enriched by miR-3666. **D** Binding sequence between miR-3666 and circ_0008315. **E** Luciferase reporter assay was used to detect luciferase activity after co-transfecting with miR-3666 mimics and circ_0008315-WT or circ_0008315-MUT reporter plasmids. **F** FISH assay showing circ_0008315 and miR-3666 were co-localized in GC cells. **G**, **H** The expression level of miR-3666 was decreased in both GC cell lines and GC tissues. **I** Circ_0008315 was negatively correlated with the expression level of miR-3666 in GC tissues. **p < 0.01; ***p < 0.001

It has been previously documented that miR-3666 inhibits EMT in lung cancer cells [16]. However, it has not been proved whether miR-3666 can exert a similar effect in GC. We added miR-3666 mimics to MKN-45 cells and then detected alterations in EMT-related markers. Western blotting and immunofluorescence showed that miR-3666 mimics incorporation resulted in an increase in E-cadherin and a decrease in N-cadherin and vimentin (Additional file 1: Fig. S4). The results showed that changes in miR-3666 could lead to varieties in EMT markers.

MiR-3666 targeted CPEB4 in GC

To validate whether circ_0008315 could sponge miR-3666 and liberate the expression of its downstream targets, we identified five target genes of miR-3666 by overlapping the prediction results of the four algorithms (starBase, PicTar, miRDB, and RNA22). We found that miR-3666 could target the 3' untranslated regions (UTRs) of KLF7, PHF20, AGFG1, PRKAA1, CPEB4, CNOT6L, SNX27, ANKIB1, and PPP6R2 (Fig. 5A). We searched for the downstream target genes of circ_0008315 by gauging the mRNA levels of nine candidate genes after circ_0008315 knockdown. We found that the expression levels of KLF7 and CPEB4 were significantly downregulated (Fig. 5B). However, overexpression of circ_0008315 in HGC-27 cells led to a higher level of CPEB4 expression than other genes (Fig. 5C). Therefore, we cloned the CPEB4 sequence of wild-type or mutant 3'UTR into luciferase reporter vector to prove whether the 3'UTR of CPEB4 mRNA was the downstream of miR-3666 by luciferase reporter assay. After adding miR-3666 mimics, the luciferase activity of GC cells transfected with CPEB4 wild-type 3'UTR sequence was significantly reduced, while the luciferase activity of GC cells transfected with mutant sequence was unchanged (Fig. 5D and E). These results suggested that miR-3666 bound to the 3'UTR of CPEB4 and directly downregulated CPEB4 expression. After transfection with miR-3666 mimics, the expression level of CPEB4 in HGC-27 and MKN-45 was

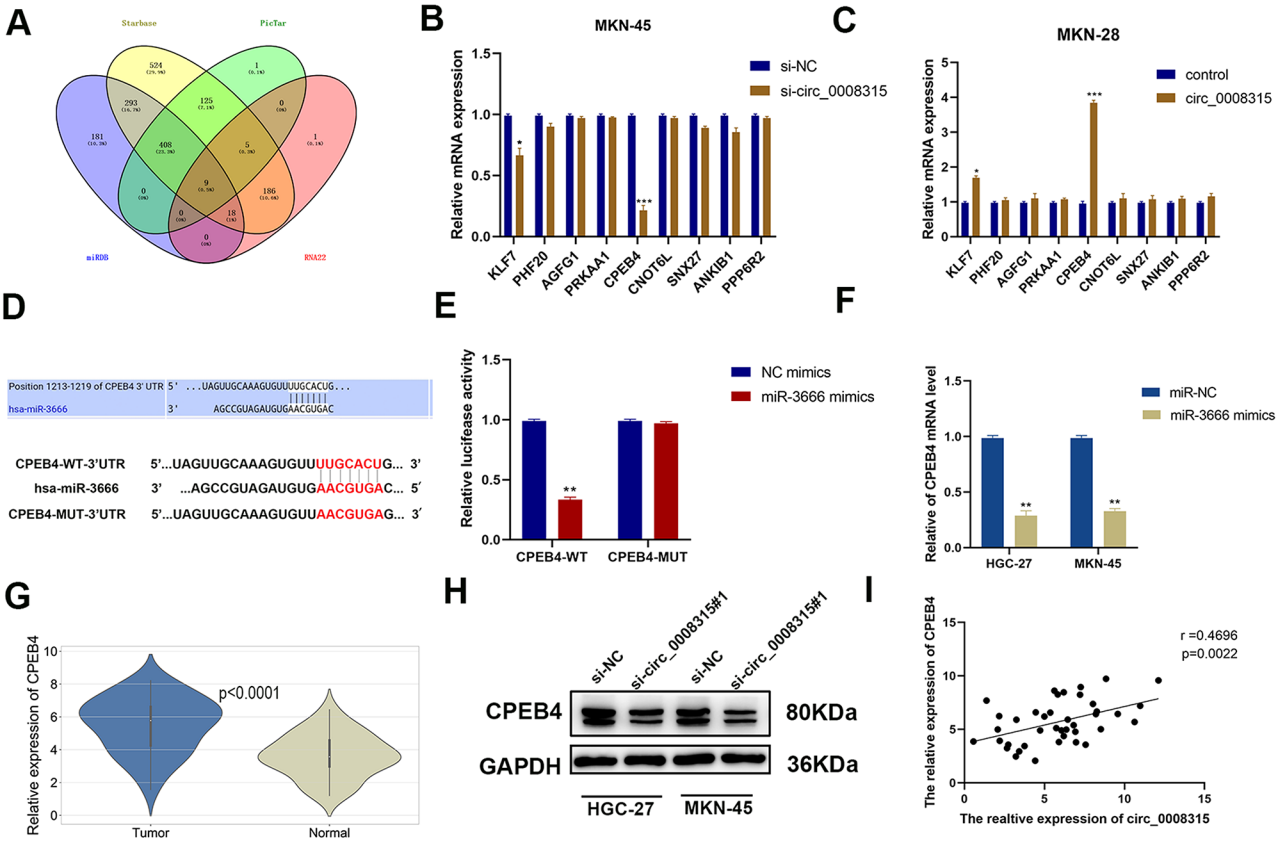

Fig. 5 MiR-3666 targets CPEB4 in GC cells. **A** Venn diagram shows the prediction of miR-3666 binding mRNAs from Starbase, PicTar, miRDB and RNA22. **B**, **C** RT-qPCR was used to detect the expression levels of downstream genes of knockdown and overexpression of circ_0008315, with the most significant changes in CPEB4; **D** predicted binding sequence of miR-3666 and CPEB. **E** Luciferase reporter gene assay was used to detect luciferase activity after co-transfecting with miR-3666 mimics and CPEB4-WT or CPEB4-MUT reporter plasmids. **F** CPEB4 expression levels were detected by RT-qPCR in MKN-45 and HGC-27 cells after transfecting with miR-3666 mimics. **G** RT-qPCR was used to detect the CPEB4 expression in GC tissues. **H** Western blotting assay was conducted to detect the CPEB4 expression level in MKN-45 and HGC-27 cells with or without circ_0008315 knockdown. **I** Circ_0008315 was positively correlated with the expression level of CPEB4 in GC tissues. *p < 0.05; **p < 0.01; ***p < 0.001

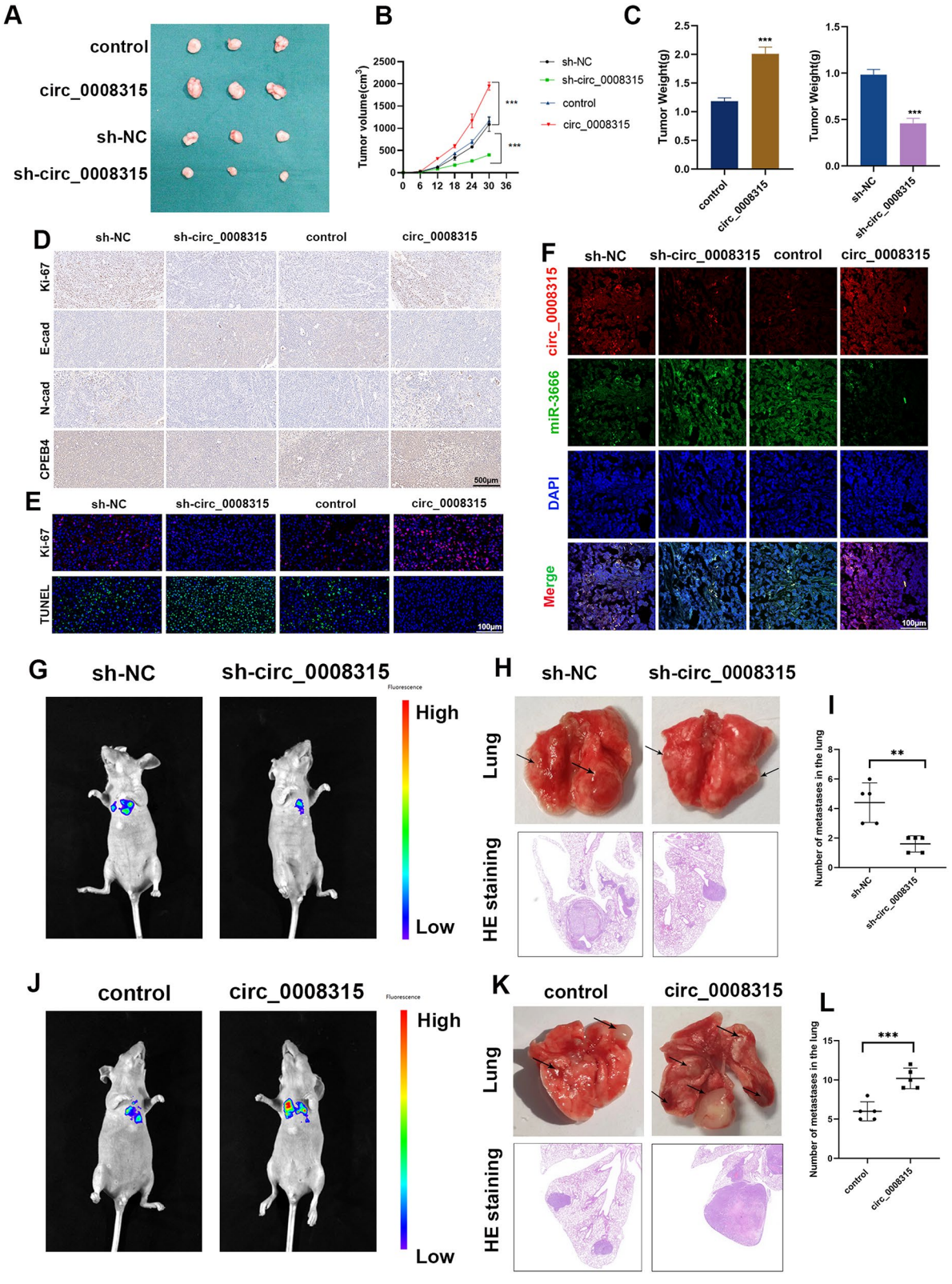

Fig. 6 (See legend on next page.)

(See figure on previous page.)

Fig. 6 Circ_0008315 facilitates GC growth and metastasis in vivo. **A** Xenograft tumors in nude mice from the four treatment groups (sh-NC, sh-circ_0008315, control, circ_0008315). **B**, **C** The volume and weight of subcutaneous xenograft tumors isolated from nude mice. **D** IHC analysis was performed to examine the expression levels of Ki-67, E-cadherin, N-cadherin and CPEB4 in xenograft tumors isolated from nude mice. **E** Ki-67 and TUNEL staining was used to detect the proliferation and apoptosis of xenograft tumors from nude mice. **F** FISH showing the colocalization and expression levels of circ_0008315 and miR-3666 in xenograft tumors isolated from nude mice. **G** Representative images of pulmonary metastatic foci in mice inoculated with MKN-45 cells with or without circ_0008315 knockdown via tail vein. **H** Specimen plots and HE staining of pulmonary metastatic foci in mice inoculated with MKN-45 cells with or without circ_0008315 knockdown. **I** The number of pulmonary metastatic foci was counted in mice inoculated with MKN-45 cells with or without circ_0008315 knockdown. **J** Representative images of lung metastasis in mice inoculated with MKN-28 cells with or without circ_0008315 overexpression via tail vein. **K** Specimen plots and HE staining of pulmonary metastatic foci in mice inoculated with MKN-28 cells with or without circ_0008315 overexpression. **L** The number of pulmonary metastatic foci was counted in mice inoculated with MKN-28 cells with or without circ_0008315 overexpression. *p < 0.05; **p < 0.01; ***p < 0.001; n = 3

decreased (Fig. 5F). We utilized RT-qPCR and validated that CPEB4 expression level was significantly upregulated in GC tissues (Fig. 5G). Western blotting results showed that circ_0008315 knockdown downregulated CPEB4 in MKN-45 and HGC-27 cells (Fig. 5H). In addition, the level of circ_0008315 was positively correlated with CPEB4 expression (Fig. 5I). These data showed that circ_0008315 promoted CPEB4 expression by interacting with miR-3666 in GC cells.

Inhibition of miR-3666 reversed the effects of circ_0008315 knockdown on GC proliferation, migration and invasion

To validate whether circ_0008315 could regulate the malignant phenotypes of GC cells by sponging miR-3666, we performed the rescue experiments using miR-3666 inhibitor. We found that knockdown of miR-3666 increased the cell viability and proliferation ability of MKN-45 and HGC-27, which were attenuated by downregulation of circ_0008315 (Additional file 1: Fig. S5A and B). Meanwhile, silencing miR-3666 could also rescue the effect of circ_0008315 inhibition on EdU-positive cells (Additional file 1: Fig. S5C and D). Downregulation of miR-3666 abolished circ_0003221 knockdown-mediated effects on cell cycle and cell apoptosis (Additional file 1: Fig. S5E and 6A). MiR-3666 downregulation abated the anti-migration effects caused by circ_0008315 knockdown (Additional file 1: Fig. S6B and C). These results suggested that circ_0008315 exerted its role by targeting miR-3666.

Knockdown of CPEB4 inhibited the effects of circ_0008315 overexpression on proliferation, migration and invasion in GC

We then explored whether the circ_0008315/miR-3666/CPEB4 axis could regulate GC malignant progression. CCK-8 results showed that CPEB4 knockdown could inhibit the effect of circ_0008315 overexpression on AGS and MKN-28 cell proliferation (Additional file 1: Fig. S7A and B). CPEB4 deletion could reduce the proportion of EdU-positive cells caused by circ_0008315 overexpression (Additional file 1: Fig. S7C and D). CPEB4 silencing downregulated the proportion of G1 phase cells with circ_0008315 overexpression (Additional file 1: Fig. S7E). Transwell assay confirmed that CPEB4 knockdown could hinder the invasion ability augmented by circ_0008315 overexpression (Additional file 1: Fig. S8A). CPEB4 deletion reduced the migratory ability increased by circ_0008315 overexpression (Additional file 1: Fig. S8B). In summary, the promoting effects of circ_0008315 on GC proliferation, migration, and invasion could be rescued by CPEB4 inhibition.

circ_0008315 facilitated GC growth and metastasis in vivo

To investigate the role of circ_0008315 in vivo, we transfected MKN-45 cells with circ_0008315 knockdown or MKN-28 cells with circ_0008315 overexpression lentiviruses and subcutaneously injected them into the inguinal region of BALB/c nude mice. The results showed that tumor growth was significantly inhibited in the sh-circ_0008315 group, and the tumors were larger and heavier after circ_0008315 overexpression (Fig. 6A-C). The expression levels of Ki-67, E-cadherin, N-cadherin, and CPEB4 were detected using immunohistochemical (IHC). The results of IHC revealed that xenograft tumors derived from MKN-28 cells with circ_0008315 overexpression had higher levels of Ki-67, N-cadherin, and CPEB4, than those in the control group. But the expression level of E-cadherin changes in the opposite direction. After the downregulation of circ_0008315, IHC in xenografts obtained the contrary results to overexpression (Fig. 6D). Similarly, fluorescence staining also confirmed that Ki-67 was significantly reduced and TUNEL was increased in xenografts with circ_0008315 knockdown, while circ_0008315 overexpression was the opposite (Fig. 6E). FISH results showed that circ_0008315 knockdown significantly elevated miR-3666 expression in tumor tissues, while circ_0008315 overexpression significantly reduced miR-3666 expression when compared with the control group (Fig. 6F).

To further confirm the invasion effects of circ_0008315 in vivo, a lung metastasis model was established by inoculating MKN-45 cells with circ_0008315 knockdown or MKN-28 cells with circ_0008315 overexpression into the tail veins of nude mice. We observed the lung metastasis of tumors by detecting luciferase signals. Obviously, the luciferase signal after knockdown of circ_0008315

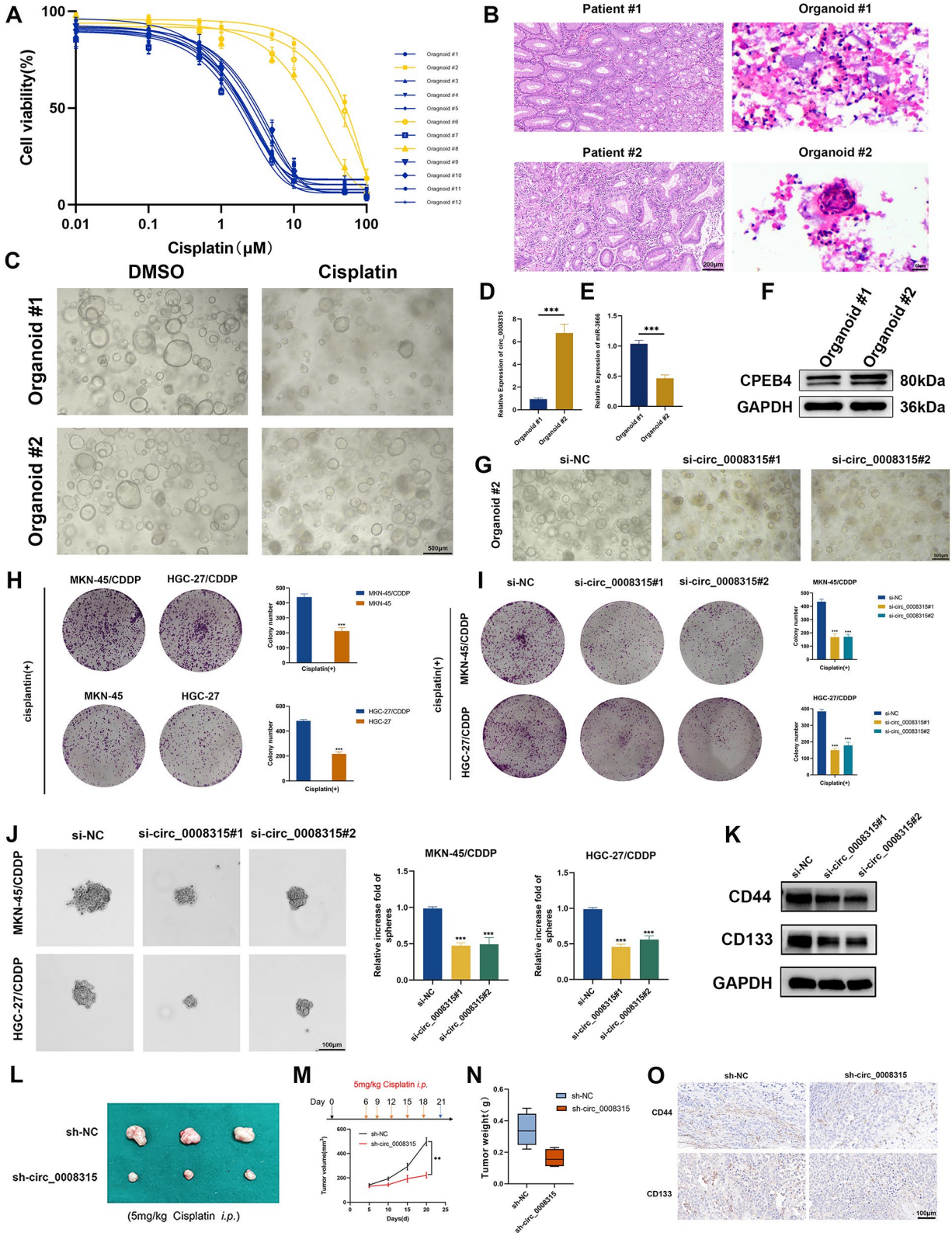

Fig. 7 (See legend on next page.)

(See figure on previous page.)

Fig. 7 Circ_0008315 enhances CDDP resistance of GC cells. **A** Drug resistance curve of organoids. **B** HE staining of GC tissues and organoids. **C** Organoids morphology after CDDP stimulation. **D** The expression levels of circ_0008315 in organoid #1 and organoid #2. **E** The expression levels of miR-3666 in organoid #1 and organoid #2. **F** Detection of CPEB4 expression between organoid #1 and organoid #2 by WB. **G** Knockdown of circ_0008315 in organoid #2 and observed the organoid morphology in the presence of CDDP. **H** In the presence of CDDP, the number of colonies of CDDP-resistant and CDDP-sensitive GC cells was detected. **I** Knockdown of circ_0008315 in CDDP-resistant cells and detection of the number of surviving cell colonies in the presence of CDDP. **J** Tumor sphere-forming assay showing smaller sphere-forming volume of drug-resistant cells after circ_0008315 knockdown. **K** Western blotting results demonstrated that CD133 and CD44 expression was decreased in MKN-45/CDDP cells after knockdown of circ_0008315. **L**-**N** In vivo drug resistance models also showed that knockdown of circ_0008315 inhibited the volume and weight of xenograft tumors. **O** Immunohistochemical detection of CD44 and CD133 expression levels in mouse xenograft tumors. *p < 0.05; **p < 0.01; ***p < 0.001; n = 3

was lower than the control group, indicating that lung metastasis was significantly restrained (Fig. 6G). Moreover, circ_0008315 knockdown inhibited the occurrence of metastatic colonization and the number of pulmonary metastatic foci (Fig. 6H and I). In contrast, circ_0008315 overexpression significantly promoted lung metastasis compared to the control group (Fig. 6J-L). Therefore, we concluded that circ_0008315 could facilitated the growth and metastasis of GC in vivo.

Circ_0008315 promotes CDDP resistance of GC cells

We collected patient tissues to construct human GC organoids, and studied the changes of circ_0008315-miR-3666-CPEB4 axis in resistant and sensitive GC organoids. We first determined whether organoids were resistant to CDDP based on the results of drug sensitivity experiments (Fig. 7A). Among the 12 organoids, most showed sensitivity to CDDP and only organoid #2, organoid #6 and organoid #8 were CDDP-resistant. Organoid #1 and organoid #2 were used for subsequent experiments. The results of HE staining showed that organoids could simulate the tumor microenvironment in vivo to a certain extent (Fig. 7B). Comparing organoid #1 and organoid #2, we observed significant differences in the growth morphology and number of the two organoids after CDDP treatment (Fig. 7C). PCR and WB results showed that in organoid #2, the expression of circ_0008315 and CPEB4 were higher than in organoid #1, while miR-3666 expression level was opposite (Fig. 7D-F). We knocked down circ_0008315 in organoid #2 and then treated it with CDDP, the therapeutic effect was significantly improved (Fig. 7G).

GO enrichment analysis suggested that the top enrichment CPEB4-associated biological processes were EMT, G protein-coupled receptor signaling pathway and response to drugs (Additional file 1: Fig. S9A). Subsequently, drug sensitivity analysis of CPEB4 revealed a higher IC50 value for CDDP in high CPEB4 expression group, suggesting that CPEB4 may promote CDDP resistance (Additional file 1: Fig. S9B). Depletion of circ_0008315 remarkably reduced the IC50 value of CDDP after inhibiting MKN-45 cells and HGC-27 cells when compared to CDDP-resistant cells. Similarly, colony formation assays revealed that the quantity of surviving cell colonies was larger in CDDP-resistant cells in the presence of CDDP (Fig. 7H). In addition, cell viability was markedly suppressed by silencing circ_0008315 in CDDP-resistant cells in the presence of CDDP (Fig. 7I). Tumor sphere-forming assay also showed that knockdown of circ_0008315 resulted in smaller sphere-forming volumes of drug-resistant cells (Fig. 7J). Western blotting results showed that knockdown of circ_0008315 resulted in reduced expression of CD133 and CD44 in MKN-45/CDDP cells (Fig. 7K). In vivo experiments also confirmed that circ_0008315 knockdown inhibited the volume and weight of the xenograft tumors subcutaneously injected by MKN-45/CDDP cells (Fig. 7L-N). IHC assay was used to verify the expression levels of stemness markers in xenograft tumors. Compared with the sh-NC group, the expression levels of CD44 and CD133 were repressed in the circ_0008315 knockdown group (Fig. 7O). These results suggested that circ_0008315 could promote CDDP resistance by regulating the stem cell properties of GC cells.

As shown in Fig. 5B and C, a change in circ_0008315 would cause a corresponding change in KLF7. To validate the effect of KLF7 on CDDP resistance in GC cells, we designed four siRNAs to knock down the expression of KLF7, si-KLF7#1 and si-KLF7#2 were able to effectively knock down KLF7 (Additional file 1: Fig. S10A). In the presence of CDDP, knockdown of KLF7 in CDDP-resistant cells did not significantly alter the number of surviving cells (Additional file 1: Fig. S10B-D).

Synthesis and characterization of PLGA-PEG(si-circ_0008315#1)NPs in vitro

We sought to develop an efficient delivery vehicle of siRNA targeting circ_0008315 as a potential therapy for GC. Abovementioned results showed that siRNA delivery could effectively knock down the expression of circ_0008315 and inhibit its effects on cell proliferation, migration, and invasion ability in vitro. It is crucial to develop approaches for siRNA delivery in vivo, since it is challenging for naked siRNA to penetrate the cell membranes [17, 18]. The double emulsion solvent diffusion method was used to prepare the PEGylated PLGA NPs loaded with si-circ_0008315#1 and spermidine, named PLGA-PEG(si-circ_0008315#1)NPs. PLGA-PEG(si-circ_0008315#1)NPs were spherical in shape and presented narrow size distributions according to

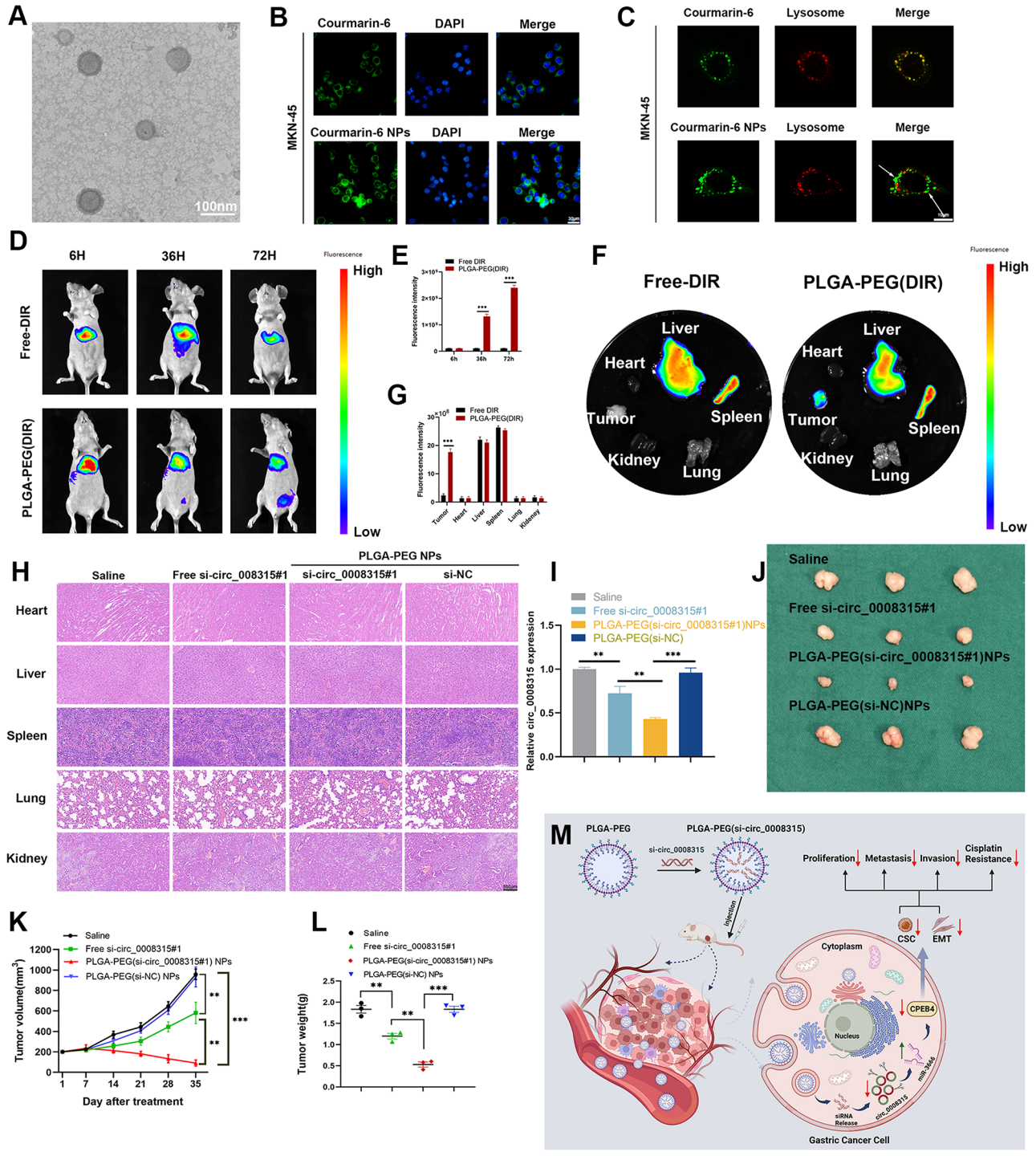

Fig. 8 Characterization and efficacy of PLGA-PEG(si-circ_0008315#1)NPs by systemic injection in CDDP-resistant model. **A** Representative TEM image of PLGA-PEG(si-circ_0008315#1) NPs. **B** Courmarin-6 assay was used to detect the effect of NPs on drug absorption in MKN-45 cells. **C** Lysosomal escape experiment was used to detect the ability of NPs to evade lysosomal degradation disruption in MKN-45 cells. **D**-**G** Targeting of PLGA-PEG nanomaterials was tested by mouse imaging in vivo and tissue imaging ex vivo. **H** HE staining showed that intravenous PLGA-PEG NPs had no significant toxicity to major organs. **I** The expression levels of circ_0008315 in xenografts was detected by RT-qPCR. **J** CDDP-resistant xenograft models were established by injecting of MKN-45/CDDP cells into the flanks of nude mice. The engrafted tumors in the Saline, Free si-circ_0008315#1, PLGA-PEG(si-circ_0008315#1)NPs and PLGA-PEG(si-NC)NPs groups were harvested. **K**, **L** The volume and weight of xenograft tumors isolated from mice. **M** Schematic diagram demonstrating the molecular mechanisms underlying circ_0008315 in GC. All experiments were repeated three times and the final results were expressed as mean ± SD. **p < 0.01; ***p < 0.001; n = 3

transmission electron microscope (Fig. 8A). The obtained PLGA-PEG(si-circ_0008315#1)NPs had a milky-white appearance in solution (Additional file 1: Fig. S11A) with a diameter of 115 nm and a negative zeta potential of -19.2 mV (Additional file 1: Fig. S11B and C). The encapsulation efficiency (EE%) of si-circ_0008315#1 was 75.27% ± 1.50%. The polydispersity index (PDI) of PLGA-PEG(si-circ_0008315#1)NPs was around 0.25 (Additional file 1: Fig. S11D). To further investigate the cellular uptake of siRNA in vitro, we incubated the cells with Courmarin-6 labeled NPs. Fluorescence microscopy results revealed that Courmarin-6 NPs exhibited a prominent fluorescent signal inside the cells compared to the control group (Fig. 8B). We also used Lyso-Tracker Red staining to observe whether PLGA-PEG(si-circ_0008315#1)NPs can reduce drug metabolism by lysosomes. Compared with the control group, the PLGA-PEG(si-circ_0008315#1)NPs group apparently reduced the degree of overlap between the drug and lysosomes (Fig. 8C). These results suggesting that the vehicle we developed could increase cellular drug uptake and reduce the clearance effect of lysosomes on drugs.

The release of si-circ_0008315#1 from PLGA-PEG(si-circ_0008315#1)NPs was also examined. The cumulative release of siRNA from free si-circ_0008315#1 and PLGA-PEG(si-circ_0008315#1)NPs was 83.3% and 44.7% after 24 h, respectively. However, at lower pH, the release of siRNA would be faster (Additional file 1: Fig. S11E). A sustained release could last for about a week. We also confirmed the knockdown efficiency of circ_0008315 in PLGA-PEG(si-circ_0008315#1)NPs in GC cells (Additional file 1: Fig. S11F). We found that the PLGA-PEG signal was mainly accumulated in the liver by tail vein injection of free DIR dye and PLGA-PEG-labelled DIR dye. PLGA-PEG-labelled DIR dye was also accumulated in mouse tumor sites, reflecting the targeting nature of the nanomaterial PLGA-PEG (Fig. 8D-G).

Efficacy of PLGA-PEG(si-circ_0008315#1)NPs by systemic injection in a patient-derived xenograft (PDX) model

GC PDX mouse models were utilized to investigate the effects of PLGA-PEG(si-circ_0008315#1)NPs on GC growth in vivo (Additional file 1: Fig. S12A). We treated the PDX model by injecting PLGA-PEG(si-NC)NPs or PLGA-PEG(si-circ_0008315#1)NPs via tail vein. Tumor growth was significantly inhibited after treatment with PLGA-PEG(si-circ_0008315#1)NPs than PLGA-PEG(si-NC)NPs (Additional file 1: Fig. S12B). The volume and weight of xenograft tumors in mice injected with PLGA-PEG(si-circ_0008315#1)NPs were significantly reduced (Additional file 1: Fig. S12C and D). Systemic toxicity was assessed by H&E staining. The results showed that intravenous administration of PLGA-PEG(si-circ_0008315#1) NPs exhibited no significant toxicity towards the liver, kidney, lung, spleen, and heart (Fig. 8H). The level of alanine transaminase (ALT), aspartate transaminase (AST), creatinine (Cr), and blood urea nitrogen (BUN) results confirmed the absence of significant hepatotoxicity and renotoxicity (Additional file 1: Fig. S12E-H). RT-qPCR results verified the consistent knockdown of circ_0008315 in xenografts derived from mice treated with PLGA-PEG(si-circ_0008315#1)NPs (Fig. 8I).

Furthermore, we generated CDDP-resistant xenograft models, gave the same CDDP treatment to explore the effect of PLGA-PEG(si-circ_0008315#1) NPs on GC CDDP-resistance in vivo. We found that the tumors were significantly reduced in the PLGA-PEG(si-circ_0008315#1)NPs group compared to the PLGA-PEG(si-NC)NPs group (Fig. 8J-L). These results demonstrated that PLGA-PEG(si-circ_0008315#1)NPs could inhibit GC growth and reverse CDDP resistance. A graphic illustration of the role of PLGA-PEG(si-circ_0008315#1)NPs in GC is depicted in Fig. 8M.

Discussion

CircRNAs are widely distributed in eukaryotic tissues, exosomes, and body fluids, and can be used as biomarkers for early diagnosis and prognostic prediction due to its high abundance and stability [19]. CircRNAs contain miRNA response elements (MREs)and can act as ceRNA to sponge miRNAs [20]. In this study, we filtered the differentially expressed circRNAs between CDDP-resistant GC cells and the parental CDDP-sensitive cells by RNA-seq. We found that circ_0008315 was highly expressed in GC tissues and CDDP-resistant GC cells. Moreover, survival analysis indicated that patients with high circ_0008315 expression had unfavorable survival outcomes.

To delineate the role of circ_0008315 in GC, we first determined the effects of circ_0008315 on tumor cell growth and metastasis in vitro. Our findings demonstrated that circ_0008315 overexpression promoted GC cell proliferation, migration, and invasion. Tumorigenic assays in nude mice confirmed that circ_0008315 promoted tumor cell growth and metastasis in vivo. Circ_0008315 was mainly located in the cytoplasm according to the nucleoplasmic separation experiments and FISH results. Thus, we explored whether circ_0008315 could target specific miRNAs and act as a miRNA sponge. Bioinformatics analysis revealed that circ_0008315 and CPEB4 both harbored miR-3666 MREs, indicating the presence of the circ_0008315/miR-3666/CPEB4 axis.

MiR-3666 has been recognized as a tumor suppressor in various cancers, including breast cancer [21], thyroid carcinoma [22], and colorectal cancer [23]. Reportedly, miR-3666 is downregulated in ovarian carcinoma cells, and miR-3666 overexpression could inhibit cell migration

and invasion and induce cell apoptosis [24]. In bladder cancer, miR-3666 targets SMAD5 to suppress cell proliferation and migration [25]. Here, we found that miR-3666 was downregulated in GC tissues and could inhibit tumor metastasis. Knockdown of circ_0008315 promoted the expression level of miR-3666, inhibiting EMT and invasion of GC cells. Moreover, miR-3666 inhibitor could reverse the suppressive effect of circ_0008315 knockdown on CDDP resistance in GC. Furthermore, luciferase reporter, RIP, and miRNA pull-down assays were performed to confirm the direct interaction between circ_0008315 and miR-3666.

Through bioinformatics analysis and expression verification, we screened CPEB4 from many downstream targets of miR-3666 for subsequent research. CPEB4 is highly correlated with tumor cell proliferation and drug resistance. CPEB4 has been found to be prominently upregulated in colorectal cancer [26], gastric cancer [27], lung cancer [28], breast cancer [29] and plays a role as a oncogene. Liu et al. reported that CPEB4 promotes CDDP resistance in esophageal cancer cells by upregulating the expression of anti-apoptotic protein Mcl-1 [30]. CPEB4 induces CSAG2 expression through translational regulation, and leads to paclitaxel resistance in ovarian cancer cells [31]. CPEB4, upregulated by lncRNA FOXD2-AS1, could promote cell proliferation, temozolomide resistance and suppress apoptosis of glioma cells [32]. In consistence with previous studies, our data showed that CPEB4 was upregulated in GC cells and tissues. Silencing of CPEB4 repressed the malignant behaviors of GC cells. The effects on GC cell biological function mediated by circ_0008315 overexpression could be reversed by CPEB4 downregulation.

CDDP resistance remains a great clinical challenge worldwide [33]. However, the mechanisms of CDDP chemoresistance remain unclear. Previous study demonstrated that circ_0017274 could facilitate CDDP resistance via regulating the miR-637/CDX2 axis in GC [34]. In this study, we demonstrated that the expression of circ_0008315 was significantly increased in CDDP-resistant GC cells. Bioinformatics results suggested that CPEB4 was associated with CDDP resistance in GC. We observed that knockdown of circ_0008315 reduced CDDP resistance in GC cells and enhanced the expression of stem cell markers CD133 and CD44. Tumor sphere formation in a suspension culture system can mimic the three-dimensional spatial conformation microenvironment of solid tumors when growing in vivo [35]. We explored performed tumor cell sphere-forming assays so as to simulate the three-dimensional environment of tumor cell in vivo. Compared to GC cells sensitive to CDDP, drug-resistant cells tended to form spheres according to tumor cell sphere-forming assays. In the GC organoids we constructed, the expression of circ_0008315 and CPEB4 increased in CDDP-resistant organoids, while the expression of miR-3666 decreased. Knockdown of circ_0008315 could partly reduce the resistance of GC organoids to CDDP. Collectively, circ_0008315 expression was upregulated and positively correlated with tumor progression and CDDP resistance. Circ_0008315 may serve as a promising predictive biomarker in GC progression and CDDP resistance.

Targeted delivery of siRNA using NPs has been considered practical and promising for cancer therapy. Liposomal and viral vectors are potential siRNA delivery vehicles, but they could cause toxicity and fail to maintain sustained siRNA release [36]. Approved by the FDA, PLGAs are biodegradable and non-toxic, with high stability, extended circulation time, and controlled release properties [37]. PEG protected NPs from plasma protein binding and reduced the amount of NPs recognized by immune. Therefore, PEGylated increases the retention time of NPs in vivo, enabled more NPs to be absorbed by tumors, and improves the bioavailability [38]. Among the various polymers developed for construction of nanoplatforms, PLGA has gained significant attention and has been applied for siRNA delivery [39, 40]. PLGA is characterized by biodegradability, non-toxicity and high stability, and PLGA-based NPs incorporating siRNA may serve as a promising nanotherapeutic strategy for the treatment of cancers.

In this study, we developed a PEGylated PLGA nanoplatform targeting circ_0008315 in GC treatment. This PLGA-based NP system is characterized with the controlled release of si-circ_0008315 and could prevent si-circ_0008315 from premature degradation. The PLGA-PEG-siRNA complex allowed the entry of si-circ_0008315 into cells without additional chemical modifications. Biocompatible PEGs can increase siRNA stability in serum and enhance cellular uptake of siRNA and tumor accumulation. Based on the results of cellular uptake assays, PLGA-PEG(si-circ_0008315#1)NPs showed enhanced uptake in tumor cells, which may promote the accumulation of PLGA-PEG(si-circ_0008315#1) NPs in tumors. PLGA-PEG(si-circ_0008315#1)NPs effectively inhibited circ_0008315 expression in GC cells and showed significant antitumor effects in animal models. Furthermore, the results of histopathological analysis and blood biochemical examination confirmed that the PLGA-PEG(si-circ_0008315#1)NPs had no significant toxic side effects.

Conclusions

We showed that circ_0008315 was an oncogenic circRNA and could serve as a prognostic biomarker for GC. Circ_0008315 sponged miR-3666 and modulated CPEB4 to promote GC progression and metastasis. Furthermore, circ_0008315 exerted a critical role in regulating the stem

cell properties of GC cells through the miR-3666/CPEB4 axis to induce chemoresistance to CDDP. We designed a novel nano platform encapsulating si-circ_0008315 for GC treatment. Our findings revealed that PLGA-PEG(si-circ_0008315#1)NPs were tumor-targeting with satisfactory antitumor efficacy. Our data may provide insights into the role of circular RNAs in cancer nanotherapeutic strategies.

Abbreviations

ALT	Alanine transaminase
AST	Aspartate transaminase
BUN	Blood urea nitrogen
CCK-8	Cell counting kit-8
CDDP	Cisplatin
ceRNA	Competing endogenous RNA
CI	Confidence intervals
circRNAs	Circular RNAs
Cr	Creatinine
DFS	Disease-free survival
DPI	Dispersibility index
EdU	5-Ethynyl-2′-deoxyuridine
EMT	Epithelial-mesenchymal transition
FBS	Fetal bovine serum
FISH	Fluorescence in situ hybridization
GC	Gastric cancer
HR	Hazard ratios
IC50	Half maximal inhibitory concentration
IF	Immunofluorescence
IHC	Immunohistochemical
miRNAs	microRNAs
MREs	miRNA response elements
NTA	Nanoparticle tracking analysis
OS	Overall survival
PBS	Phosphate-buffered saline
PDX	Patient-derived xenograft
RIP	RNA immunoprecipitation
RT-qPCR	Quantitative real-time polymerase chain reaction
shRNAs	Small hairpin RNAs
UTRs	Untranslated regions

Supplementary Information

The online version contains supplementary material available at https://doi.org/10.1186/s12951-024-02760-6.

Supplementary Material 1

Supplementary Material 2

Acknowledgements
Not applicable.

Author contributions
X.W., X.Z. and J.C. initiated the project. Y.F., D.C., X.Z. and J.C. designed the study. D.C. and R.D. performed the bioinformatics analyses. Y.F., D.C., Y.L. and Z.W. performed the experiments. Y.L., M.Z. and P.G. collected clinical specimens. Y.F. and D.C. wrote the manuscript. Y.F. and X.Z. reviewed the manuscript. J.C. and X.Z. provided fundings. All authors read and approved the final manuscript.

Funding
This work was supported by the Natural Science Foundation of Anhui Education Department for Distinguished Young Scholars (2022AH020074), the Natural Science Foundation of Anhui Education Department for Excellent Young Scholars (2022AH030123), the Support Plan for Outstanding Young Talents of Anhui Education Department (gxyq2021257), the Natural Science Research Project of Higher Education Institutions of Anhui Education Department (2023AH040254), the Provincial Quality Engineering Project of Anhui Education Department (2022jyxm1722 and 2022jyxm1733) and the Talent Introduction Science Foundation of Yijishan Hospital, Wannan Medical College (YR202109 and YR202110).

Data availability
No datasets were generated or analysed during the current study.

Declarations

Competing interests
The authors declare no competing interests.

Author details
[1]Department of Gastrointestinal Surgery, The First Affiliated Hospital, Yijishan Hospital of Wannan Medical College, Wuhu 241001, China
[2]Department of Hepatobiliary Surgery, The First Affiliated Hospital, Yijishan Hospital of Wannan Medical College, Wuhu 241001, China
[3]Anhui Province Key Laboratory of Non-coding RNA Basic and Clinical Transformation, Wannan Medical College, Wuhu 241001, China
[4]Department of Oncology, The First Affiliated Hospital, Yijishan Hospital of Wannan Medical College, Wuhu 241001, China

Received: 14 April 2024 / Accepted: 6 August 2024
Published online: 29 August 2024

References

1. Sung H, Ferlay J, Siegel RL, et al. Global Cancer statistics 2020: GLOBOCAN estimates of incidence and Mortality Worldwide for 36 cancers in 185 countries. CA Cancer J Clin. 2021;71:209–49.
2. Van Cutsem E, Sagaert X, Topal B, Haustermans K, Prenen H. Gastric cancer. Lancet. 2016;388:2654–64.
3. Yuan L, Xu ZY, Ruan SM, Mo S, Qin JJ, Cheng XD. Long non-coding RNAs towards precision medicine in gastric cancer: early diagnosis, treatment, and drug resistance. Mol Cancer. 2020;19:96.
4. Wang X, Xu Z, Sun J, et al. Cisplatin resistance in gastric cancer cells is involved with GPR30-mediated epithelial-mesenchymal transition. J Cell Mol Med. 2020;24:3625–33.
5. Galluzzi L, Senovilla L, Vitale I, et al. Molecular mechanisms of cisplatin resistance. Oncogene. 2012;31:1869–83.
6. Yang Q, Li F, He AT, Yang BB. Circular RNAs: expression, localization, and therapeutic potentials. Mol Ther. 2021;29:1683–702.
7. Huang S, Yang B, Chen BJ, et al. The emerging role of circular RNAs in transcriptome regulation. Genomics. 2017;109:401–7.
8. Tang X, Ren H, Guo M, Qian J, Yang Y, Gu C. Review on circular RNAs and new insights into their roles in cancer. Comput Struct Biotechnol J. 2021;19:910–28.
9. Tao M, Zheng M, Xu Y, Ma S, Zhang W, Ju S. CircRNAs and their regulatory roles in cancers. Mol Med. 2021;27:94.
10. Huang A, Zheng H, Wu Z, Chen M, Huang Y. Circular RNA-protein interactions: functions, mechanisms, and identification. Theranostics. 2020;10:3503–17.
11. Deng G, Mou T, He J, et al. Circular RNA circRHOBTB3 acts as a sponge for mir-654-3p inhibiting gastric cancer growth. J Exp Clin Cancer Res. 2020;39:1.
12. Huang X, Li Z, Zhang Q, et al. Circular RNA AKT3 upregulates PIK3R1 to enhance cisplatin resistance in gastric cancer via miR-198 suppression. Mol Cancer. 2019;18:71.
13. Wu D, Xia A, Fan T, Li G. circRASGRF2 functions as an oncogenic gene in hepatocellular carcinoma by acting as a miR-1224 sponge. Mol Ther Nucleic Acids. 2021;23:13–26.
14. Li B, Wang W, Li Z, et al. MicroRNA-148a-3p enhances cisplatin cytotoxicity in gastric cancer through mitochondrial fission induction and cyto-protective autophagy suppression. Cancer Lett. 2017;410:212–27.
15. Lo YH, Kolahi KS, Du Y, et al. A CRISPR/Cas9-Engineered ARID1A-Deficient human gastric Cancer Organoid Model reveals essential and nonessential modes of Oncogenic Transformation. Cancer Discov. 2021;11:1562–81.
16. Pan L, Tang Z, Pan L, Tang R. MicroRNA-3666 inhibits lung cancer cell proliferation, migration, and invasiveness by targeting BPTF. Biochem Cell Biol. 2019;97:415–22.
17. Bobbin ML, Rossi JJ. RNA interference (RNAi)-Based therapeutics: delivering on the Promise? Annu Rev Pharmacol Toxicol. 2016;56:103–22.

18. Huang Y, Hong J, Zheng S, et al. Elimination pathways of systemically delivered siRNA. Mol Ther. 2011;19:381–5.
19. Yang L, Wilusz JE, Chen LL. Biogenesis and Regulatory roles of Circular RNAs. Annu Rev Cell Dev Biol. 2022;38:263–89.
20. Kristensen LS, Andersen MS, Stagsted LVW, Ebbesen KK, Hansen TB, Kjems J. The biogenesis, biology and characterization of circular RNAs. Nat Rev Genet. 2019;20:675–91.
21. Li D, Li L. MicroRNA–3666 inhibits breast cancer cell proliferation by targeting sirtuin 7. Mol Med Rep. 2017;16:8493–500.
22. Wang G, Cai C, Chen L. MicroRNA-3666 regulates thyroid Carcinoma Cell Proliferation via MET. Cell Physiol Biochem. 2016;38:1030–9.
23. Yang D, Li R, Xia J, Li W, Zhou H. miR–3666 suppresses cellular proliferation and invasion in colorectal cancer by targeting SATB2. Mol Med Rep. 2018;18:4847–54.
24. Tan H, Wu C, Huang B, Jin L, Jiang X. MiR-3666 serves as a tumor suppressor in ovarian carcinoma by down-regulating AK4 via targeting STAT3. Cancer Biomark. 2021;30:355–63.
25. Ke H, Zhang J, Wang F, Xiong Y. ZNF652-Induced circRHOT1 Promotes SMAD5 Expression to Modulate Tumorigenic Properties and Nature Killer Cell-Mediated Toxicity in Bladder Cancer via Targeting miR-3666. J Immunol Res. 2021; 2021: 7608178.
26. Zhong X, Xiao Y, Chen C, et al. MicroRNA-203-mediated posttranscriptional deregulation of CPEB4 contributes to colorectal cancer progression. Biochem Biophys Res Commun. 2015;466:206–13.
27. Cao G, Chen D, Liu G, Pan Y, Liu Q. CPEB4 promotes growth and metastasis of gastric cancer cells via ZEB1-mediated epithelial- mesenchymal transition. Onco Targets Ther. 2018;11:6153–65.
28. Hu J, Zhang L, Chen Q, et al. Knockdown of CPEB4 expression suppresses cell migration and invasion via akt pathway in non-small cell lung cancer. Cell Biol Int. 2018;42:1484–91.
29. Lu R, Zhou Z, Yu W, Xia Y, Zhi X. CPEB4 promotes cell migration and invasion via upregulating vimentin expression in breast cancer. Biochem Biophys Res Commun. 2017;489:135–41.
30. Liu Z, Gu S, Wu K, et al. CircRNA-DOPEY2 enhances the chemosensitivity of esophageal cancer cells by inhibiting CPEB4-mediated Mcl-1 translation. J Exp Clin Cancer Res. 2021;40:361.
31. Zhang Y, Gan H, Zhao F, et al. CPEB4-Promoted Paclitaxel Resistance in Ovarian Cancer in Vitro relies on Translational Regulation of CSAG2. Front Pharmacol. 2020;11:600994.
32. Gu N, Wang X, Di Z, et al. Silencing lncRNA FOXD2-AS1 inhibits proliferation, migration, invasion and drug resistance of drug-resistant glioma cells and promotes their apoptosis via microRNA-98-5p/CPEB4 axis. Aging. 2019;11:10266–83.
33. Miao YH, Mao LP, Cai XJ, et al. Zinc oxide nanoparticles reduce the chemoresistance of gastric cancer by inhibiting autophagy. World J Gastroenterol. 2021;27:3851–62.
34. Xu B, Guo J, Chen M. Circ_0017274 acts on miR-637/CDX2 axis to facilitate cisplatin resistance in gastric cancer. Clin Exp Pharmacol Physiol. 2022;49:1105–15.
35. Chen Y, Zhang Z, Henson ES, et al. Autophagy inhibition by TSSC4 (tumor suppressing subtransferable candidate 4) contributes to sustainable cancer cell growth. Autophagy. 2022;18:1274–96.
36. Sousa AR, Oliveira AV, Oliveira MJ, Sarmento B. Nanotechnology-based siRNA delivery strategies for metastatic colorectal cancer therapy. Int J Pharm. 2019;568:118530.
37. Dawidczyk CM, Kim C, Park JH, et al. State-of-the-art in design rules for drug delivery platforms: lessons learned from FDA-approved nanomedicines. J Control Release. 2014;187:133–44.
38. Devulapally R, Foygel K, Sekar TV, Willmann JK, Paulmurugan R. Gemcitabine and Antisense-microRNA co-encapsulated PLGA-PEG polymer nanoparticles for Hepatocellular Carcinoma Therapy. ACS Appl Mater Interfaces. 2016;8:33412–22.
39. Zhou B, Mo Z, Lai G, et al. Targeting tumor exosomal circular RNA cSERPINE2 suppresses breast cancer progression by modulating MALT1-NF-κB-IL-6 axis of tumor-associated macrophages. J Exp Clin Cancer Res. 2023;42:48.
40. Zuo X, Chen Z, Gao W, et al. M6A-mediated upregulation of LINC00958 increases lipogenesis and acts as a nanotherapeutic target in hepatocellular carcinoma. J Hematol Oncol. 2020;13:5.

Publisher's Note